THESIS

NEUTRON PRODUCTION AND TRANSPORT AT A MEDICAL LINEAR ACCELERATOR

Submitted by

Amber Allardice

Department of Environmental and Radiological Health Sciences

In partial fulfillment of the requirements

For the Degree of Master of Science

Colorado State University

Fort Collins, Colorado

Summer 2014

Master's Committee:

Advisor: Alexander Brandl

James Custis
James Lindsay

ABSTRACT

NEUTRON PRODUCTION AND TRANSPORT AT A MEDICAL ACCELERATOR

The Colorado State University Veterinary Teaching Hospital (VTH) uses a Varian Trilogy™ linear accelerator (linac) for radiation oncology treatment. The high-energy electron beam is used to treat superficial tumors (deep tissues are spared with this modality) or is accelerated against a target to produce high-energy photons that are used to treat deep seated tumors (skin is spared with this modality). Either application might exceed the neutron production threshold for various materials. This study evaluates neutron production and transport in the environment surrounding the VTH trilogy through MCNP modeling and physical measurements of the 10 MV photon and 18 MeV electron beam modalities.

MCNP modeling was accomplished in two phases. The first phase involved simulating the linear accelerator and determining the relevant parameters for neutron production for both modalities. This was accomplished by using various target specifications and replicating the geometry of the machine. In the second phase, MCNP modeling of the accelerator vault as well as other locations of interest within the treatment suite was conducted. This phase determined measurable neutron fluence and dose rates at the test locations where physical measurements were taken. The MCNP results (for neutron energies between 0.2 to 10 MeV) were compared with the physical measurements. Physical measurements were performed with a BF_3 detector (responsive to energies between 0.2 and 10 MeV) and taken at the same test locations.

For both modalities, MCNP and physical measurements demonstrated neutron production. Large uncertainties were associated with the physical measurements for both

modalities. For the photon mode, MCNP modeling resulted in neutron equivalent doses per photon Gy up to 0.112 mrem/photon Gy, and physical measurements up to 0.133 mrem/photon Gy. For the electron mode, MCNP modeling resulted in measureable neutron equivalent doses per electron Gy up to 14.88 mrem/electron Gy, and physical measurements up to 3.83×10^{-04} mrem/electron Gy. Taking the entire neutron spectrum into account, MCNP results showed neutron doses up to 347.81 mrem/ photon Gy at the isocenter for the photon beam, and up to 1.77×10^{5} mrem/electron Gy at the isocenter for the electron beam. These numbers could not be compared to the physical measurements because the BF_3 detector used in this experiment only responded to neutron energies between 0.2 and 10 MeV. The conclusion made from this research is that neutrons are generated at various locations in and outside the room. For the photon modality, the neutron dose to the patient can be considered negligible when compared with the treatment dose. Neutron production does not appear to exceed the tolerance for workers in appropriate locations surrounding the VTH linac vault. Further research is recommended for an accurate analysis of both modalities.

ACKNOWLEDGEMENTS

First, thanks to Dr. Alexander Brandl, my advisor, for all of your help with this project. Your time and dedication to making sure I understood concepts and MCNP in particular is much appreciated. This paper would not be a success without your involvement!

Next, thanks to several other people for this time and dedication in helping me with the MCNP modeling and physical experiment portions of this research. Thanks specifically to Rafe McBeth for running some of my MCNP simulations on the cluster when they got too long for me to run on my one little processor. Special thanks to Dr. James Custis for staying after work late into the night to help me take physical measurements. Also, thanks to Dr. Thomas Johnson for lending me the Logitech camera and to the Colorado State University Radiation Safety Staff for lending me your BF_3 detector.

Last, and certainly not least, thanks to all my family and friends for encouraging me to stick with this project in the challenging moments and for putting up with my talks even though I would lose you at "photoneutron". I especially want to thank my parents, Robert and Susan Allardice, for all of your love, guidance and support not just through this project, but throughout my life. You are the role models I live by!

TABLE OF CONTENTS

LIST OF TABLES

LIST OF FIGURES

Introduction

The Veterinary Teaching Hospital (VTH) at Colorado State University (CSU) in Fort Collins, Colorado uses a Varian Trilogy linear accelerator (linac) to treat spontaneously arising tumors in animal patients. The VTH Trilogy offers two modalities of external beam radiotherapy (EBRT)-high energy x-rays (a.k.a photons) and electrons. Both modalities can be operated at energies that have the potential to produce neutrons. One of the goals in radiotherapy is to avoid doses from radiation (i.e. neutrons that contaminate the therapeutic beam) that provide no therapeutic benefit, but may result in potential side effects or secondary malignancies in the future. The purpose of this research is to evaluate neutron production and transport at the VTH Trilogy linac and to ultimately evaluate neutron contribution to patient and worker dose.

Medical Linear Accelerator Function and Components

Medical linear accelerators are used to treat various tumors by accelerating charged particles to high energies through a linear tube. The outcome is an external beam directed at a specified location-the tumor. For the purposes of this paper and the function of this linac, the charged particle of interest is the electron. The high energy electron beam, as narrow as a tip of a pencil (~ 3 mm), exits the accelerator tube and travels through several components of the linac before reaching the patient (Khan, 2010).

In photon mode, a target (typically made tungsten or copper) is placed in the electron beam path, and an energy distribution of photons is generated and used to treat deep seated tumors. This is possible, because a dose build up occurs with a maximum dose at a depth several cm below the patient's surface as photons penetrate tissue, and then gradually decreases as the photons are attenuated in the tissue. The depth at which the maximum dose is achieved increases with increasing energies. For a 10 MV photon beam, the maximum dose falls at a depth of 2.4

cm in tissue and 40-50% of the percent depth dose is at a depth of 20 cm. Because the skin is spared somewhat as the maximum dose is deeper in the tissue, the photon modality is ideal for treating deep tumors. In the electron mode, the target is retracted and the electron beam is the primary source of dose to the patient. As electrons are charged particles and have mass, they are stopped more readily at the surface instead of penetrating deeply into tissue, thus making this modality ideal for treating superficial structures while sparing the deeper organs and tissues. In

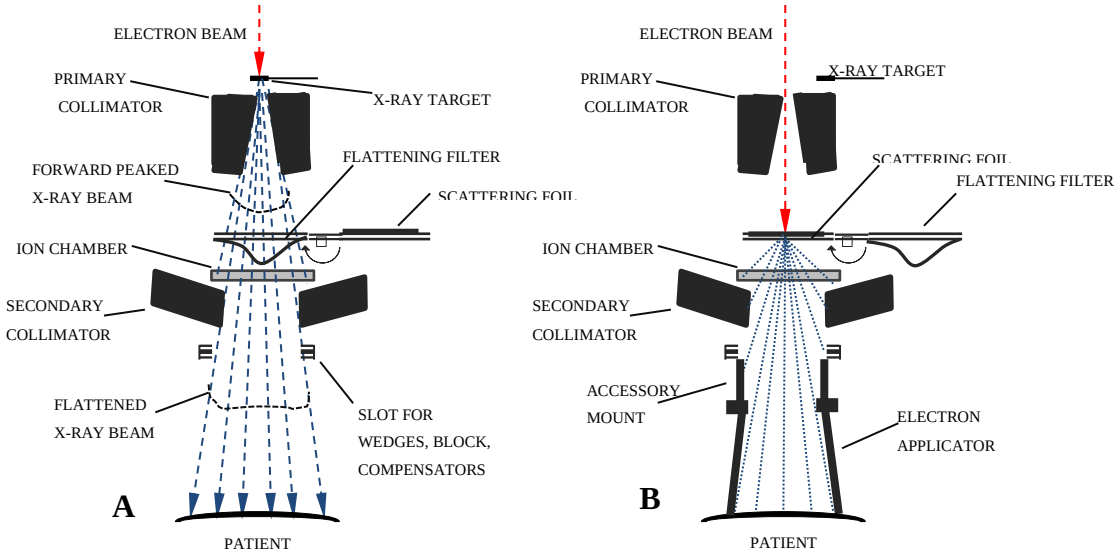

Figure 1. Components of a linac head. A: Photon mode B: Electron mode

either case, as can be seen in Figure 1, several components between the source (electron beam) and the patient are used to normalize, collimate, and shape the beam. The components are listed in Table 1. These components, as will be discussed later, play an important role in contributing to neutron production, and the material of the components is an important factor.

Table 1. Linac components

X-ray Mode	Electron Mode
X-ray target	No Target
Primary collimator	Primary collimator
Flattening filter	Scattering foil
Ion chamber	Ion chamber
Secondary collimator	Secondary collimator
Compensators	Accessory mount/Electron Applicator

The secondary collimator for both modalities consists of jaws (and upper and lower set) made of tungsten that are used to collimate the beam down to a specific square field size. Multileaf-collimators (MLCs), which are multiple thin sheets of tungsten used in intensity modulated radiation therapy (IMRT) for the photon modality, are positioned beneath the jaws. IMRT is a technique in which doses are delivered to the patient from multiple positions to maximize the dose to the tumor while sparing the surrounding healthy tissue. The purpose of the MLCs is to further shape the beam into a very detailed geometry that fits the tumor like a puzzle, allowing for dose painting to the tumor in IMRT. The MLCs are only used with the photon modality. Because of the material (tungsten) and the thickness of the secondary collimators, these components play a significant role in neutron production.

Neutron Production

At the fundamental level, an atom is made up of a certain number of neutrons and protons (nucleons) clustered together in the nucleus surrounded by a "cloud" of electrons orbiting around the nucleus. The nucleons are held together via nuclear force fields, and there is a separation energy associated with each nucleon required to separate them from the nucleus. This energy is distinct for the proton and neutron, and is much higher for the proton because of the coulomb barrier that must be overcome. Table 2 lists the threshold energies for several materials (Johnson and Birky, 2012).

Table 2. Threshold energies for photoneutron production

Isotope	Energy Threshold (MeV)
C-12 (Carbon)	18.72
O-16 (Oxygen)	15.66
Al-27 (Aluminum)	13.06
Fe-56 (Iron)	11.2
Cu-63, Cu-65 (Copper)	10.85, 9.91
W-184 (Tungsten)	7.41
Pb-208 (Lead)	7.37

Once this threshold is reached, a neutron can be emitted. There are two ways this can be accomplished: 1) via photodisintegration (γ,n) and 2) electrodisintegration (e,n). In photodisintegration, a photon interacts with the nucleus of the atom (A) and induces a photonuclear event: $\gamma + A \rightarrow (A - 1) + n$. Neutrons produced from (γ,n) reactions are called photoneutrons. In electrodisintegration, an electron is the source of the nuclear event: $e + A \rightarrow (A - 1) + n + e'$ (NCRP, 1984). In either case, two important considerations arise in neutron emission: 1. the energy of the neutron and 2. the probability of the neutron being emitted, for there is a cross-section (the probability of an interaction occurring) associated with neutron production. The cross section for (e,n) is much smaller than the cross section for (γ,n) by a factor of about 100 (Hendee et al., 2013), thus this paper will primarily focus on photoneutron production.

As previously mentioned, the x-ray beam consists of an energy distribution of photons (a.k.a the bremsstrahlung spectrum), and is a result of high-speed electrons hitting a high-Z material. The atomic number, Z, defines an element, and is the number of protons in the nucleus. The bremsstrahlung spectrum ranges from very low energies up to a maximum energy equal to the initial energy of the incident electron (Khan, 2010). For example, a 10 MeV electron will produce a 10 MV bremsstrahlung spectrum (a.k.a 10 MV photon beam). In the case of the VTH Trilogy, electrons hit the target and the photon beam is emitted on the downstream side in a

forward direction (as illustrated earlier in figure 1) due to the high energy of the incident electron.

In the electron mode, the electron beam is bent with a magnet in lieu of the target and the electron beam strikes an electron scattering foil. The purpose of the foil is to spread the electron beam and produce a uniform fluence for treatment (Khan, 2010). In the electron scattering process, a small fraction of x-ray contamination via bremsstrahlung is produced. Bremsstrahlung can also be produced by scattered electrons hitting the collimator walls and other components of the collimator system. Thus, there are several possible sources of neutron production while in electron mode.

Neutron Characterization

Neutrons fall under three categories based on their energies. Neutrons with energies below 0.5 eV are referred to as thermal neutrons, with the most probable kinetic energy at 0.025 eV. Intermediate-energy neutrons are next in line, ranging from 0.5 eV to 10 keV. Neutrons above 10 keV are fast neutrons (Attix, 2004). All neutrons are "born" fast (Cember and Johnson, 2009), and then slow down as they interact with matter via scattering (elastic and/or inelastic) and are ultimately absorbed by the material (i.e. hydrogen atoms in concrete walls) with which they interact. For this reason, though fast neutrons are expected as a result of bremsstrahlung interactions with the various linac components, potentially thermal and intermediate neutrons are added to the neutron distribution. The neutron type becomes important in neutron dosimetry, as the energy of the neutron is the determining factor in absorbed dose.

Neutron Dosimetry

Tissue consists mainly of hydrogen (H), oxygen (O), carbon (C), and nitrogen (N). The dose contribution from thermal neutrons originates from two important interactions with tissue:

$^{14}N(n,p)^{14}C$ and $^{1}H(n,\gamma)^{2}H$ (Cember, 2009). A majority of the dose is from the (n,γ) interaction as the composition for H in the body is over three times that of N (Cember and Johnson, 2009). The dose contribution from fast neutrons is from elastic collisions with hydrogen nuclei, resulting in recoil protons. The energy from the recoil protons is absorbed locally as mentioned above (Attix, 2004). The deposited energy is dependent on the energy of the neutron that results in the recoil, and thus increases with neutron energy. For this reason, the quality factor rises drastically with fast neutrons. The quality factor (also referred to as a radiation weighting factor in more updated references) is a value assigned the units rem/rad (or Sv/Gy for the radiation weighting factor) used in health physics to quantify how damaging the radiation is. Table 3 shows the quality factors designated for different neutron energies.

Table 3. ICRP 21 Quality Factors for various neutron energies

Neutron Energy (MeV)	Quality Factor
2.5×10^{-8}	2.3
1.0×10^{-7}	2.0
1.0×10^{-6}	2.0
1.0×10^{-5}	2.0
1.0×10^{-4}	2.0
0.001	2.0
0.01	2.0
0.1	7.4
0.5	11.0
1.0	10.6
2.0	9.3
5.0	7.8
10.0	6.8
20.0	6.0

An important quantity to introduce at this point is the dose equivalent (or equivalent dose in newer references), which is expressed in rem (or Sv for equivalent dose). Dose equivalent is a product of the absorbed dose (rad or Gy) and the quality factor (Turner, 2007). The reason the older units, rem and rad are discussed in addition to the more current units, is because the

computer modeling and instrumentation used for this research provide output in the older units. This also explains the quality factors used in Table 3 instead of the current radiation weighting factors provided in ICRP 60 and 103.

Previous Works

Over the decades, research on neutron production at medical accelerators has been conducted, however the focus remains on photon therapy at much higher energies (above 10 MV), and hardly any focus has been directed to electron beam therapy. The reason for this is the low expectation of neutrons being detected as well as the difficulties and limitations that exist in neutron measurements and simulations (NCRP, 1984).

Of the few publications (see Table 4) on 10 MV photon therapy, neutron fluence and doses have been evaluated at various conditions (i.e. different field sizes, etc.) and with different measurement devices (i.e. activation foils and bubble dosimeters). Additionally, as seen in Table 4, some values are reported in absorbed dose or dose equivalent, and some results in neutron yield or fluence, thus caution should be used when comparing the results between manuscripts.

Table 4. Literature Review

Authors	Experiment Conditions	Results
Deye and Young, 1977 (from NCRP)	100 cm from isocenter[a] (IC) in the patient plane; measurements made with bare activation foils	$1.0x10^{-4}$ rem/photon rad and $1.0x10^{-5}$ rad/photon rad at IC
McGinley and Sohrabi, 1979 (from NCRP)	30 cm from IC in the patient plane; measurements made with moderate activation foils	$3.8x10^{3}$ n/cm^2
McGinley et al., 1976 (from NCRP, 1984)	10 cm from IC in the patient plane; measurements made with moderate activation foils	$6.03x10^{-5}$ rad/photon rad at IC ($1.9x10^{5}$ n/cm^2)
Oliver, 1976 (from NCRP)	15 cm from IC in the patient plane; measurements made with silicon diodes	$6.30x10^{-5}$ rad/photon rad
Rogers and VanDyke, 1981 (from NCRP)	100 cm from IC in the patient plane; measurements made with activation foils in remmeter moderators	$4.00x10^{-5}$ rem/photon rad
Liu et al., 1997	Assessed neutron yields/starting particle with EGS4-MORSE/MCNP code (Jaws Closed) at various accelerator head components and neutron yield at the isocenter per photon Gy	Target: $1.7x10^{-9}$ n/s Primary collimators: $5.9\ x10^{-6}$ n/s Flatten filter: $4.5x10^{-9}$ n/s Jaws: $7.3x10^{-6}$ n/s IC: $3.8x10^{10}$ n/ photon Gy
Catchpole, 2010	Assessed neutron dose at different field sizes (at isocenter) from VMAT[b] and IMRT via MCNP modeling and Bubble Dosimeter measurements	MCNP: 0.487-18.339 mSv/photon Gy Bubble Dosimeters: 0.51-2.46 mSv/photon Gy

a. The isocenter is a reference point located on the plane perpendicular to the beam axis at a distance predetermined by the manufacturer; typically 100 cm from the target. (Khan, 2010)
b. Volume modulated arc therapy (VMAT) is a technique that also uses MLCs to shape the beam, but delivers the dose over a range of angles that create an arc (Catchpole, 2010)

Purpose revisited

The VTH Trilogy linac is capable of producing 6 and 10 MV photon beams, and a range of energies from 4-18 MeV electron beams. The 10 MV x-ray beam and energies above 8 MeV for the electron beam meet the threshold for photoneutron generation. The probability of generation is much lower for the electron beam as compared to the x-ray beam; however,

potential for neutron generation still exists because of the bremsstrahlung that can be produced as electrons interact with the various linac components (i.e. jaws). The concern is that neutrons contaminate the beam and potentially add to the patient's dose as well as to occupational exposure. The question regarding the VTH linac is whether photoneutrons are produced and in numbers sufficient to contribute to non-negligible doses. The aim of this research is to answer this question through, first, MCNP modeling and, second, physical measurements.

Materials and Methods

MCNP Simulations

The Monte Carlo N-Particle (MCNP) versions X and 5 computer codes were used for the Monte Carlo simulations. MCNP provides powerful capabilities to model simple to advanced geometries as well as production and transport of various particles (X-5 Monte Carlo Team, 2003). For this research, the particles transported were electrons, photons, and neutrons. Ultimately, evaluation of neutron fluence (number of neutrons/ cm^2) and dose equivalent (rem) were the main goals in these simulations. These values were compared with physical measurements conducted in the course of this study and also with published results. Visual Editor (VISED) version 22S was used to display the geometry models and visualize the particle transport.

The simulated linac model (see Figure 2) was based on data provided in the Varian Monte Carlo Data Package for the High Energy Accelerator (Varian Medical Systems, 2013). Figure 3 shows a simulated model of the room surrounding the linac. A series of simulations were conducted with first the 10 MV photon beam and then the 18 MeV electron beam. The simulations were conducted with and without the surrounding room (including the floor and ceiling). Table 5 shows a breakdown of the various simulations that were modeled and a brief description of each.

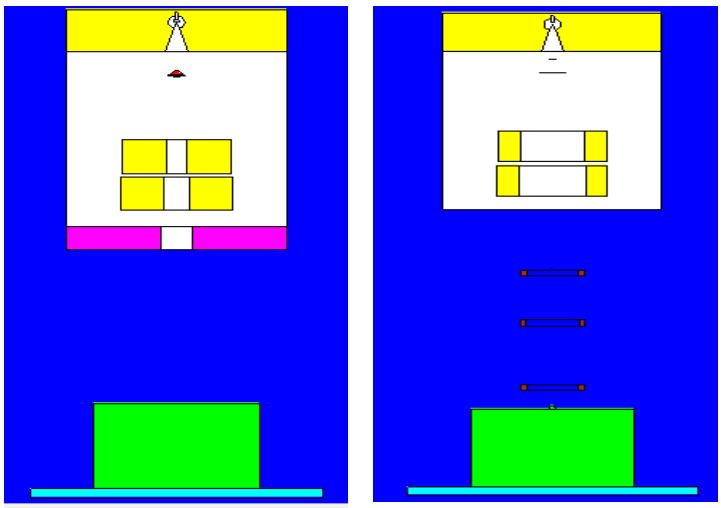

Figure 2. MCNP model of the VTH Trilogy and phantom. A: Photon mode. B: Electron mode.

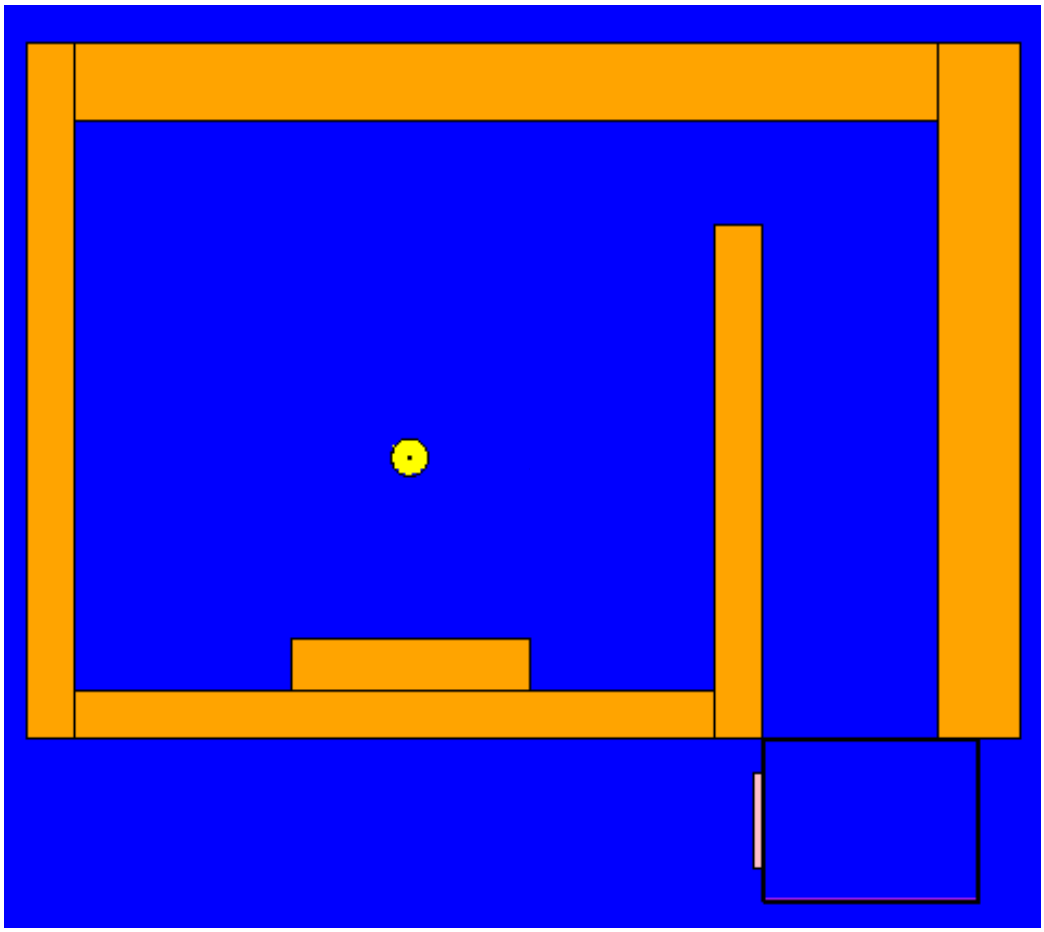

Figure 3. Diagram of VTH linac vault and maze

Table 5. MCNP Simulations

Simulation	Source Particle	Tally Type	Description/Purpose of simulation
1. Electron beam hitting various target thicknesses	10 MeV Electron beam	F1[a] and F2[b] tally for photons	Electron beam accelerated at various target thicknesses. Purpose is to validate the photon beam generated in Simulation 2 and used in Simulations 3 and 4
2. Electron beam hitting Cu target	10 MeV Electron beam	F1 tally for photons	To determine the bremsstrahlung spectrum at the target
3. 10 MV photon beam transported from target to phantom	10 MV Bremsstrahlung Spectrum (derived from Simulation 2)	F1 for neutrons	To determine neutron yield at the linac components.
4. 10 MV photon beam transported from target to phantom	10 MV Bremsstrahlung Spectrum (derived from simulation 2)	a. F5[c] tally (fluence only) for neutrons b. F5[d] tally (dose conversion factors applied) for neutrons	a. To determine fluence at components and locations in and outside room (listed in Table 6). b. To determine dose at IC and locations listed in Table 6.
5. Electron beam modality	18 MeV beam	F1 for neutrons	To determine neutron yield at the linac components.
6. Electron beam modality	18 MeV beam	a. F5 tally (fluence only) for neutrons b. F5 tally with flux-to-dose conversion for neutrons	a. To determine fluence at components and locations in and outside room (listed in Table 6). b. To determine dose at IC and locations listed in Table 6.

a. The F1 tally integrates the current over a surface. The output is in number of particles ("yield")/s per starting particle/s (X-5 Monte Carlo Team, 2003).
b. The F2 tally averages the flux (a.k.a fluence) over a surface. The output is in number of particles/cm^2/s per starting particle/s (X-5 Monte Carlo Team, 2003).
c & d. The F5 tally provides the flux at a point detector. The output is in particles/cm^2/s per starting particle/s. This tally also provides a flux-dose-conversion to rem/h (X-5 Monte Carlo Team, 2003).

The photon beams generated in Simulation 1 were benchmarked with similar spectra in the literature (Tsechanski et al., 1998) to validate the photon beam produced in the MCNP modeling. Figure 4 shows the photon beams generated for Simulation 1 with a 10 MeV pencil electron beam accelerated towards Cu targets of various thicknesses. Just as in the literature (Tsechanski et al., 1998), the photon beams peak and shift at the appropriate energies for a 10 MeV electron beam hitting a Cu target for a specific thickness. An important note to make is that the absolute values are different in the literature spectra. This is most likely due to the bin sizes used. The bin sizes selected for Simulation 1 ranged from 0.01 to 0.1 MeV (in 0.18 keV increments), 0.1 to 1.0 MeV (in 1.8 keV increments), and 1.0 to 10 MeV (in 18 keV increments).

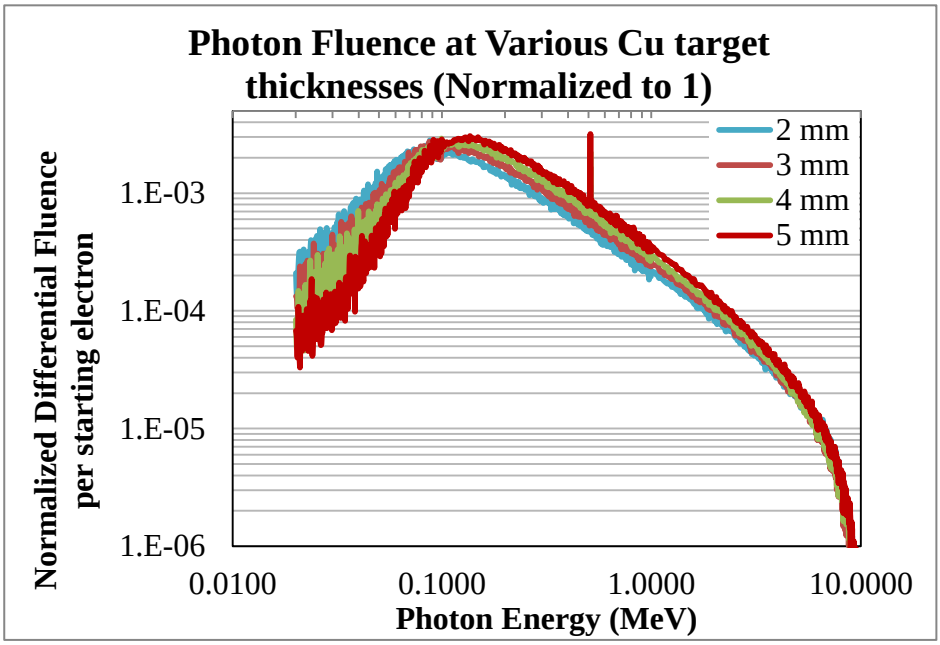

Figure 4. Photon beams generated for Simulation 1.

With the energy spectrum validated, Simulations 2-4 were conducted for the photon modality. Appendix A shows the source definition used for the photon beam, and the energy probabilities and biasing selected based on the electron beam source results. Biasing was

selected for the upper range as these energies are at or above the threshold for neutron production.

Next, two simulations (5-6) were modeled for the electron modality to evaluate the production of neutrons. For the electron model, the target, filter and MLCs are removed, and the scattering foil and electron cone applicator are added. Additionally, the phantom is positioned with a source to skin distance of 100 cm, so that the isocenter falls at the phantom surface instead of at a depth of 10 cm in tissue.

Physical Experiment

The physical experiment was conducted in the CSU VTH vault where the Varian Trilogy linac is located as well as in surrounding rooms and on the roof directly above the linac. Figure 5 shows a diagram of the vault and the rooms surrounding it as well as the positions measured (except for the roof). Table 6 gives a description of each position.

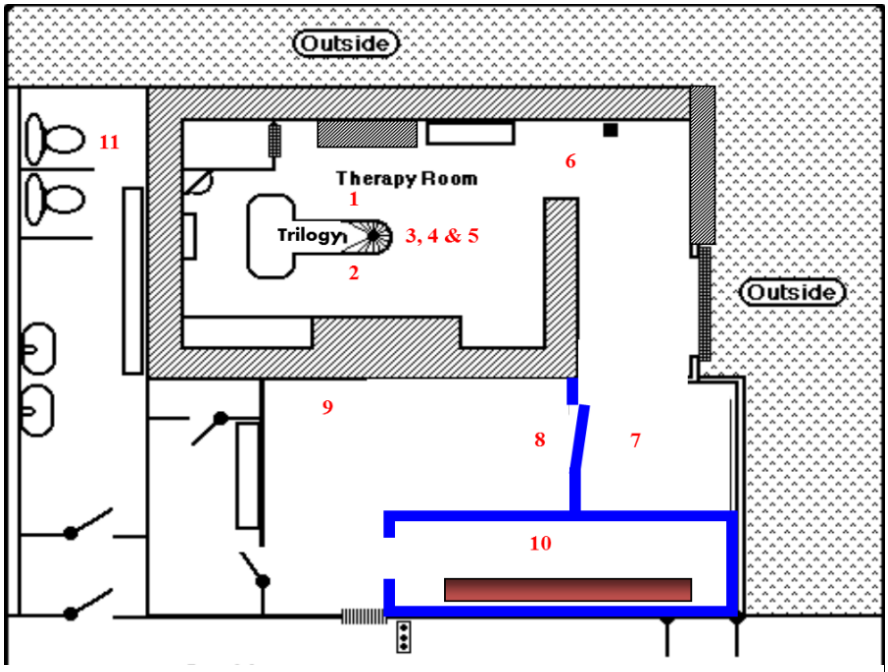

Figure 5. VTH linac room schematic and measurement locations

Table 6. Measurement Locations

Location	Description	Location	Description
1	100 cm from the target, (right side of gantry level of target; west wall side)	7	Vault door entrance (maze side)
2	100 cm from the target (left side of gantry at level of target; east wall side)	8	Vault door entrance (patient holding area; west wall)
3	40 cm from the Isocenter (away from gantry, perpendicular to beam)	9	Patient holding area (west wall)
4	60 cm from the Isocenter (away from gantry, perpendicular to beam)	10	Control Room (operator position)
5	100 cm from the Isocenter (away from gantry, perpendicular to beam)	11	Restroom (north west corner)
6	Maze entrance	12	Roof (directly above gantry)-not shown in schematic

The detector (see Figure 6) used in this experiment was a Ludlum Neutron Dose Rate Meter Model 12-4 (Serial No. 118950) supplied by the Radiation Safety Office at CSU. The calibration certificate for this instrument can be found in Appendix B. This meter contains a BF_3 detector, which makes it an ideal candidate for neutron detection because of the ^{10}B which has a neutron capture (n,α) cross section of 3840 barns. The reaction that occurs is $^{10}B(n,\alpha)\,^{7}Li$ (Cember and Johnson, 2009), and the ionizations produced from the alpha that results from this reaction are measured. The number of ionizations measured is proportional to the number of neutrons that interact with the detector. Thus, the neutrons are indirectly measured.

Figure 6. Ludlum Neutron Dose Rate Meter

Because the BF_3 is calibrated with an AmBe source which has a different energy spectrum than the neutrons produced at the linear accelerator, an energy correction must be applied to the measured values for both the photon and electron beam modes. The response curve provided by Ludlum used to determine the correction can be found in Appendix C. Based on the energy spectra derived from the MCNP results, response curves for the neutron spectra at the linac were compared to the AmBe source as seen in Figure 7. Based on these curves, a correction factor of 0.023 was determined for the 10 MV photon beam, and 0.049 for the 18 MeV electron beam. A detailed analysis of how the correction factors were derived can be found in Appendix D.

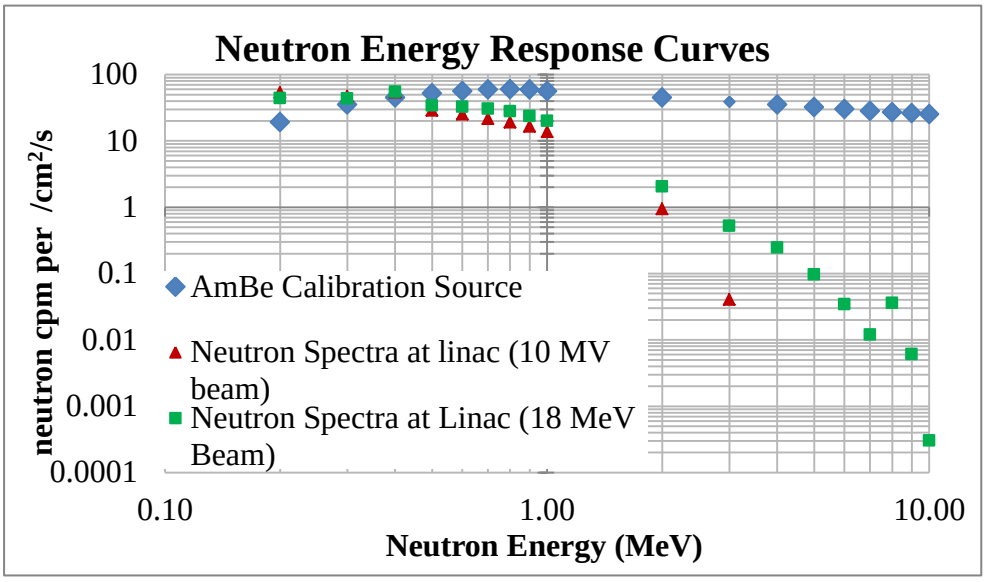

Figure 7. Comparison of energy responses for the Ludlum Model 12-4

Gamma (a.k.a photon) interference is another correction that must be applied to the measurements with this neutron dose rate meter. Where there are neutrons present, a photon field exists as well. It makes sense that the photon field is much greater than the neutron field as it is the source of the neutrons (for both the photon and electron beam) as well as the source for treatment to the patient with the photon beam. For the BF_3, as seen in Appendix B, there is gamma interference of <10 cpm for dose rates at 10 R/h. Thus, the assumption is made that there is a linear relationship between the gamma count rate and dose rate with a slope of 1. For the physical measurements, the expected excess neutron count rate due to gamma interference is subtracted from the initial count rate that is measured with the meter. Based on NCRP guidelines (Cember and Johnson, 2009), the assumption was made that 0.5% of the treatment dose rate (600 cGy/min for VTH linac) is the maximum leakage at locations 1 and 2, and 0.2% of the treatment dose rate is the maximum leakage at locations 3-5. At locations 6-12, the

assumption is made that only scatter is the contribution from gamma at this point because these locations are far enough from the linac and/or are outside the vault. MCNP was used to determine the dose rate from scatter at all locations. The sum of the leakage and scatter components are accounted for in the overall correction.

After regular clinical hours, the machine was programmed to deliver 100 cGy to the isocenter first with the 10 MV photon beam and then with the 18 MeV electron beam. For both cases, the gantry angle was set to 0 degrees, the field size at the isocenter was 10 x 10 cm^2, and a 30 x 30 x 20 cm^3 tissue equivalent phantom was placed on the table at the same location as a patient would be. For the 10 MV beam, the isocenter fell at a depth of 10 cm (source to skin distance of 90 cm) in tissue and for the 18 MeV beam, the isocenter fell right at the surface of the phantom (source to skin distance of 100 cm). To deliver a dose of 100 cGy at the isocenter with a dose rate of 600 cGy/min, 114 MU (Monitoring Unit) was selected for the photon beam and 118 MU was selected for the electron beam. The beam on time to deliver theses doses was essentially the same for both modalities-11.4 sec. The neutron meter was placed at each location and three measurements each were taken for the 10 MV mode and the 18 MeV mode. As personnel were not permitted to be in the vault during beam on time, a Logitech TM camera was set up to record the meter readings. The entire process took seven hours and a total of 66 readings were obtained (33 for the photon beam and 33 for the electron beam). Figures 8-13 show examples of the set up for the physical experiment.

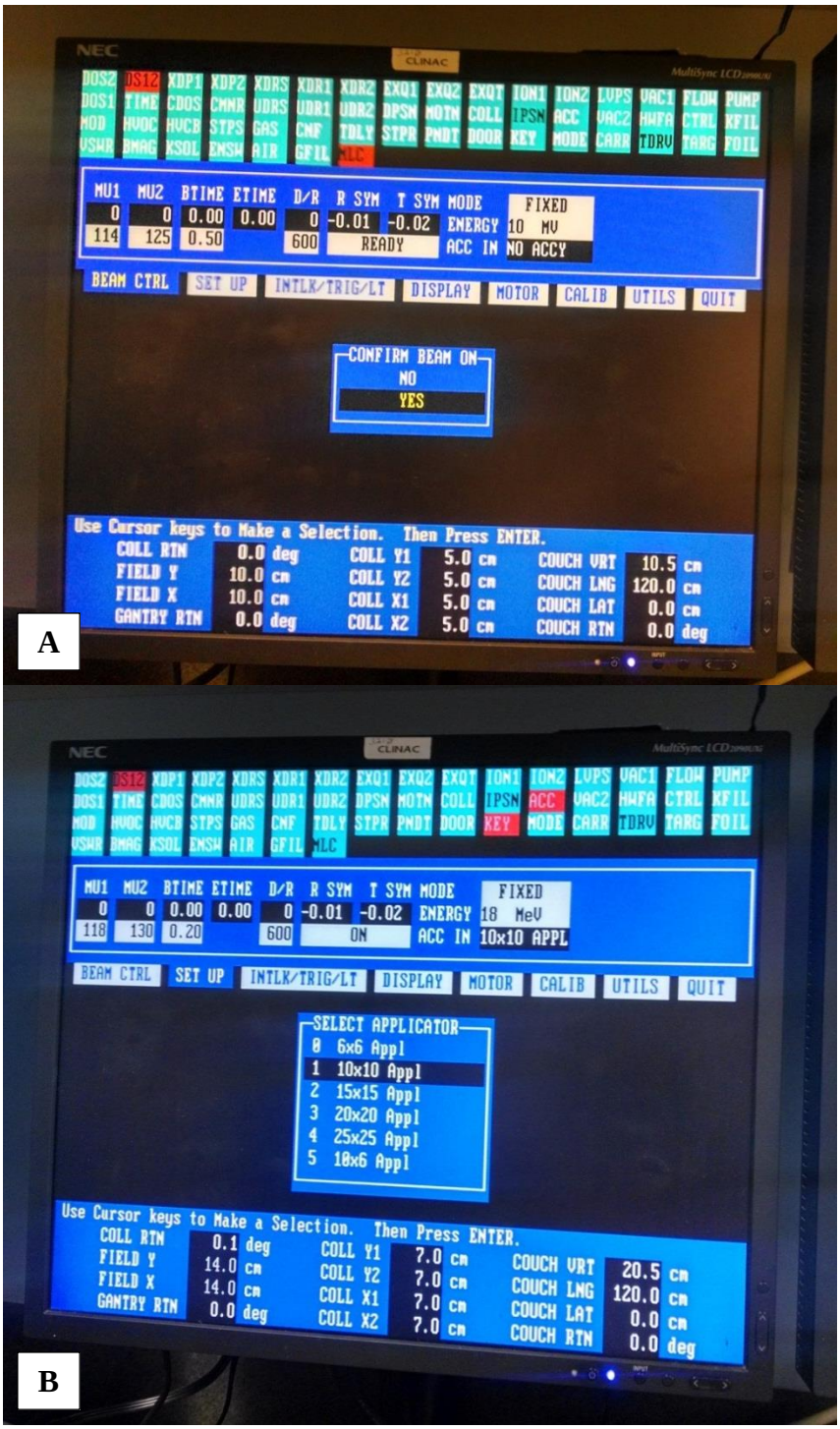

Figure 8. Physical measurement set up.
A: Console set up for photon mode B: Console set up for electron mode.

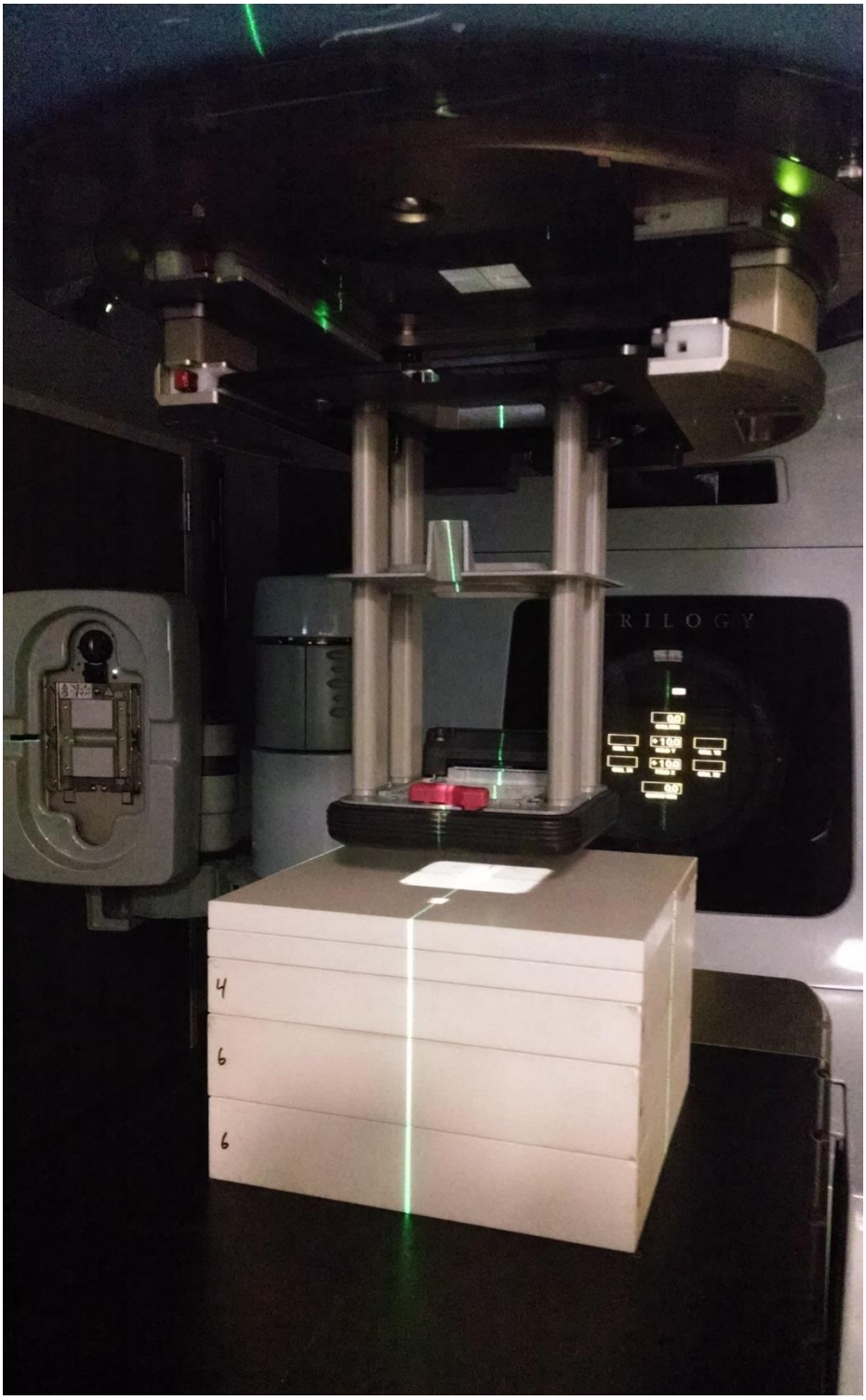

Figure 9. Physical measurement set up for electron mode

Figure 10. Physical measurement set up at Location 1 (photon mode).

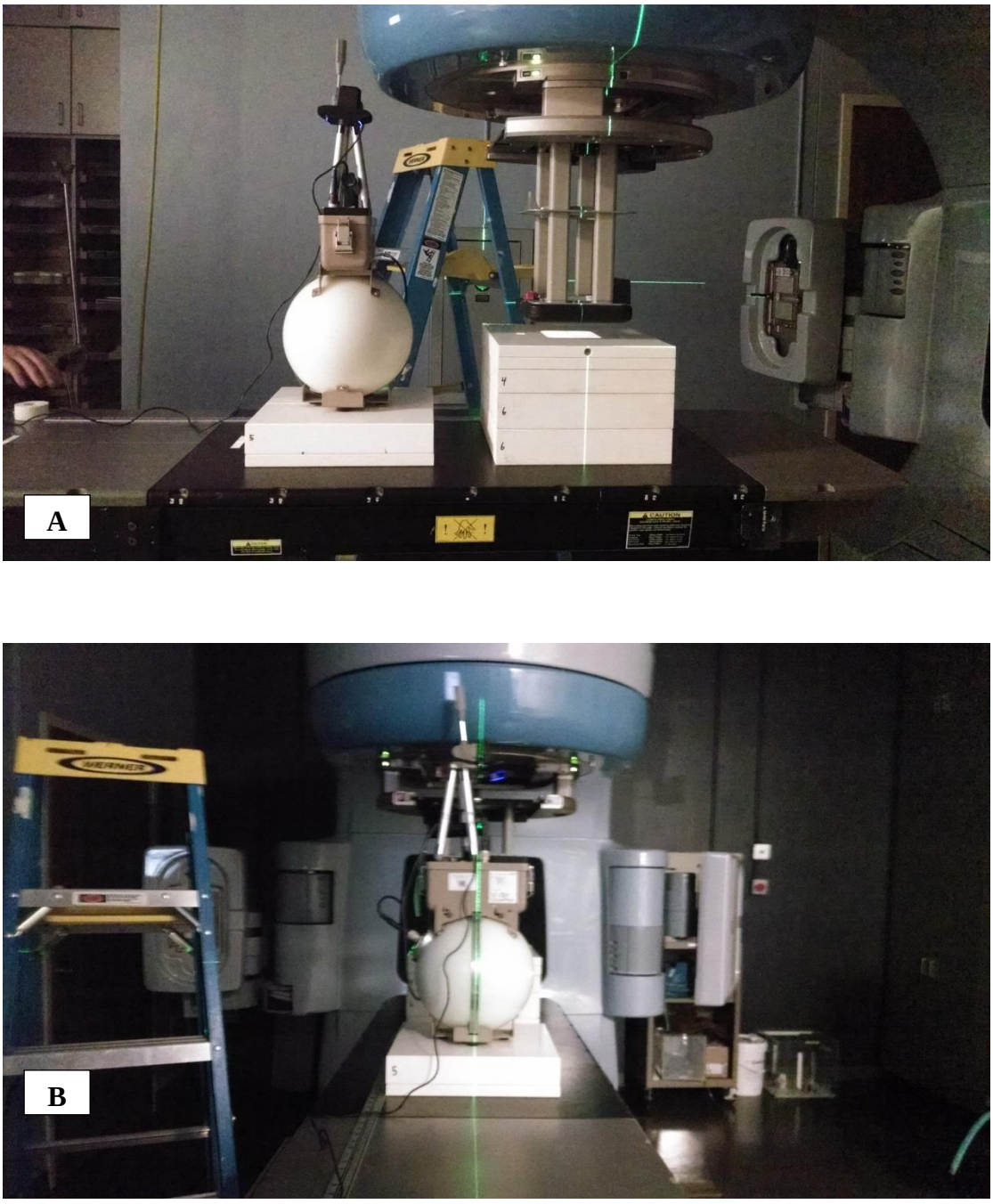

Figure 11. Physical measurement set up at Location 3 (electron mode).
A: Side view. B: Front view

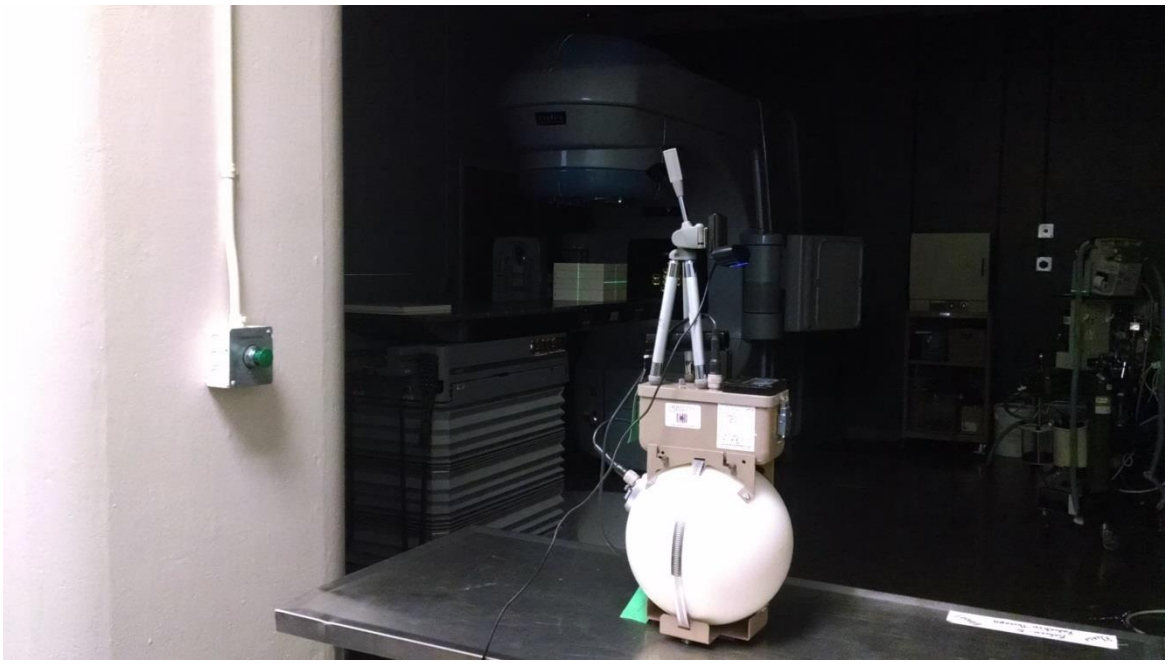

Figure 12. Physical measurement set up at Location 6.

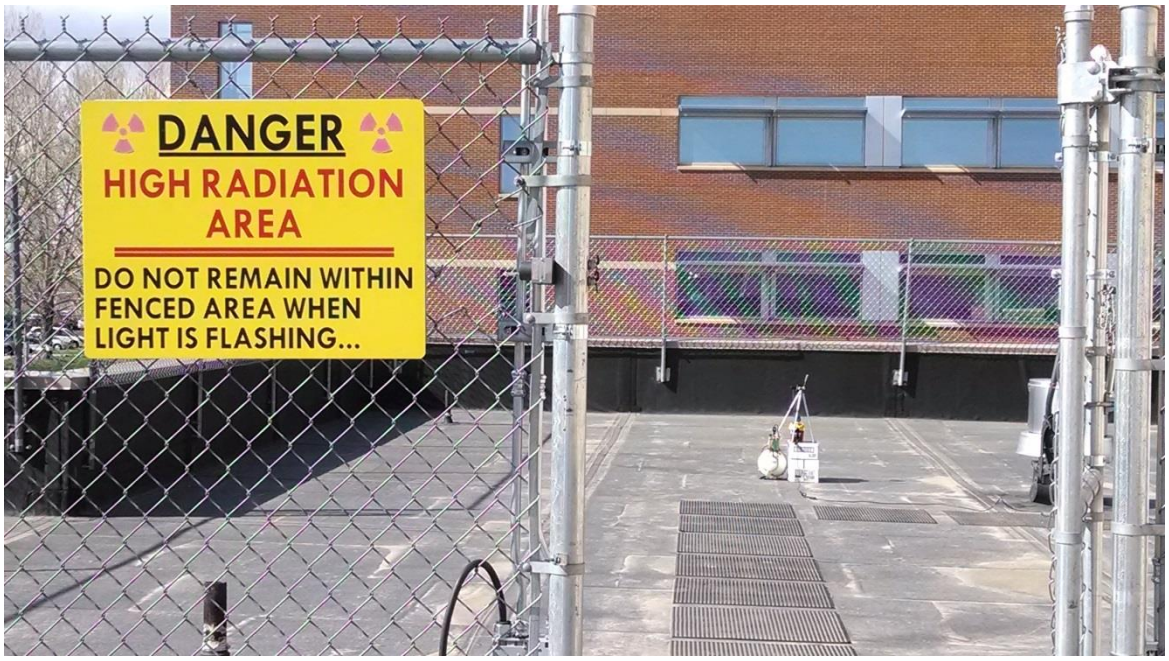

Figure 13. Physical measurement set up at Location 12.

Results

For both modalities, MCNP results are first reported per starting particle/s, as this is the output provided by MCNP for each tally. Next, using the current provided by Varian and the beam on time, the results for Simulations 4 and 6 are normalized to photon Gy (for the 10 MV beam) and electron Gy (for the 18 MeV beam) delivered at the isocenter. In the literature, this method is used for reporting neutron fluence and dose rates. For the physical measurements, results are reported in dose rate and the dose is normalized per photon Gy (or electron Gy) in the analysis and discussion when compared to the MCNP results.

MCNP Photon Beam Simulation

Table 7 summarizes the neutron yield/s at the selected linac components for the photon mode and Figure 14 shows the neutron energy spectrum obtained. Table 8 summarizes the neutron fluence and dose rates at the point detectors selected for Simulation 4 and Table 9 shows these results normalized to photon Gy at the isocenter. The location numbers listed in Tables 8 and 9 are point detectors representative of the same positions as listed in Table 6 where the physical measurements were taken. Figure 15 summarizes the neutron energy spectra for Simulation 4.

Table 7. Simulation 3 Results

Linac Component (Material)	Neutron Yield/s per Starting Electron/s	MCNP Relative Error
Target (Cu)	5.13×10^{-10}	0.050
Primary Collimator (W)	2.39×10^{-7}	0.002
Flattening Filter (Cu)	8.66×10^{-9}	0.017
Jaws (W)	1.03×10^{-6}	0.003
MLCs (W)	1.01×10^{-8}	0.004

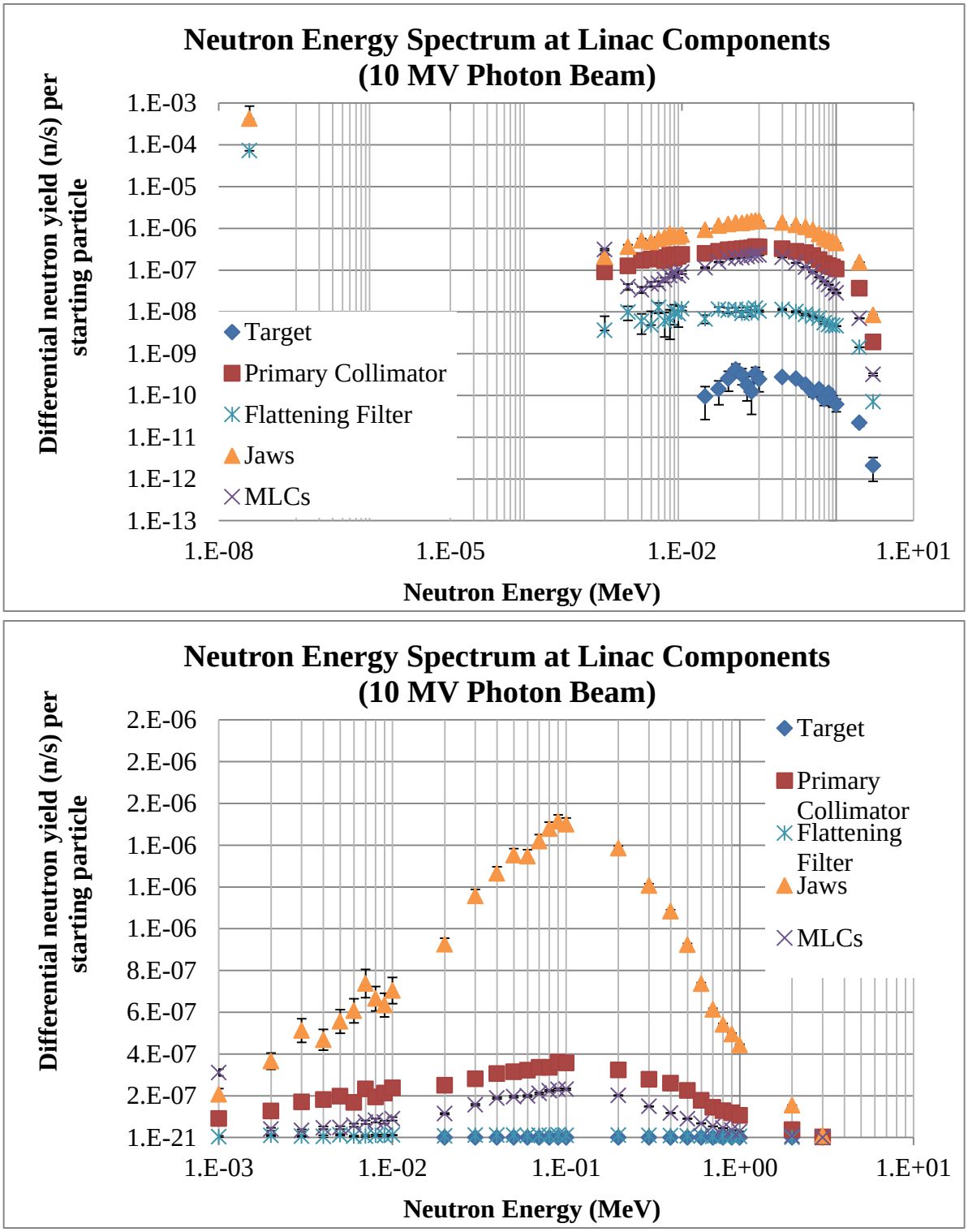

Figure 14. Simulation 3 neutron spectrum.
Entire spectrum (Top). Spectrum excluding thermal energy portion (Bottom)

Table 8. Simulation 4 Results

Location	Neutron Fluence (n/cm^2)/s per starting electron/s	Relative Error	Neutron Dose Rate (mrem/h) per starting electron/s	Relative Error
Locations below include the linac and phantom in the model only				
Isocenter (IC)	2.72×10^{-12}	0.233	1.84×10^{-14}	0.154
Location 1	3.89×10^{-12}	0.002	2.50×10^{-13}	0.002
Location 2	3.91×10^{-12}	0.002	2.52×10^{-13}	0.003
Location 3	2.40×10^{-12}	0.005	1.21×10^{-13}	0.004
Location 4	3.06×10^{-12}	0.003	1.78×10^{-13}	0.004
Location 5	2.55×10^{-12}	0.002	1.57×10^{-13}	0.003
Location 6	1.66×10^{-13}	0.003	1.08×10^{-14}	0.003
Location 12	6.59×10^{-14}	0.003	3.91×10^{-15}	0.004
Locations below include the surrounding room in the model				
Isocenter (IC)	4.04×10^{-12}	0.247	4.54×10^{-14}	0.180
Location 1	7.32×10^{-12}	0.002	2.91×10^{-13}	0.002
Location 2	7.84×10^{-12}	0.002	3.01×10^{-13}	0.002
Location 3	6.23×10^{-12}	0.002	1.75×10^{-13}	0.005
Location 4	6.81×10^{-12}	0.005	2.29×10^{-13}	0.004
Location 5	6.01×10^{-12}	0.003	1.97×10^{-13}	0.002
Location 6	1.72×10^{-12}	0.004	2.56×10^{-14}	0.005
Location 7	2.02×10^{-14}	0.050	9.85×10^{-17}	0.041
Location 8	2.30×10^{-15}	0.336	7.77×10^{-18}	0.164
Location 9	2.66×10^{-16}	0.089	1.36×10^{-18}	0.510
Location 10	3.09×10^{-15}	0.060	1.76×10^{-17}	0.061
Location 11	1.14×10^{-16}	0.481	1.22×10^{-18}	0.566
Location 12	5.34×10^{-19}	0.427	1.23×10^{-21}	0.406

Table 9. Normalized to photon Gy delivered at the isocenter

Location	Neutron Fluence (n/cm^2) per photon Gy	Neutron Dose (mrem) per photon Gy
Locations below include the linac and phantom in the model only		
Isocenter (IC)	8.72×10^6	16.38
Location 1	1.25×10^7	222.47
Location 2	1.25×10^7	223.64
Location 3	7.69×10^7	107.83
Location 4	9.81×10^6	157.96
Location 5	8.16×10^6	139.82
Location 6	5.33×10^5	9.60
Location 12	2.11×10^5	3.48
Locations below include the surrounding room in the model		
Isocenter (IC)	1.29×10^7	40.38
Location 1	2.34×10^7	259.12
Location 2	2.51×10^7	267.67
Location 3	1.99×10^7	155.71
Location 4	2.18×10^7	203.71
Location 5	1.92×10^7	175.05
Location 6	5.51×10^6	22.75
Location 7	6.47×10^4	0.088
Location 8	7370	0.007
Location 9	850	0.001
Location 10	9900	0.016
Location 11	364	0.001
Location 12	1.71	0

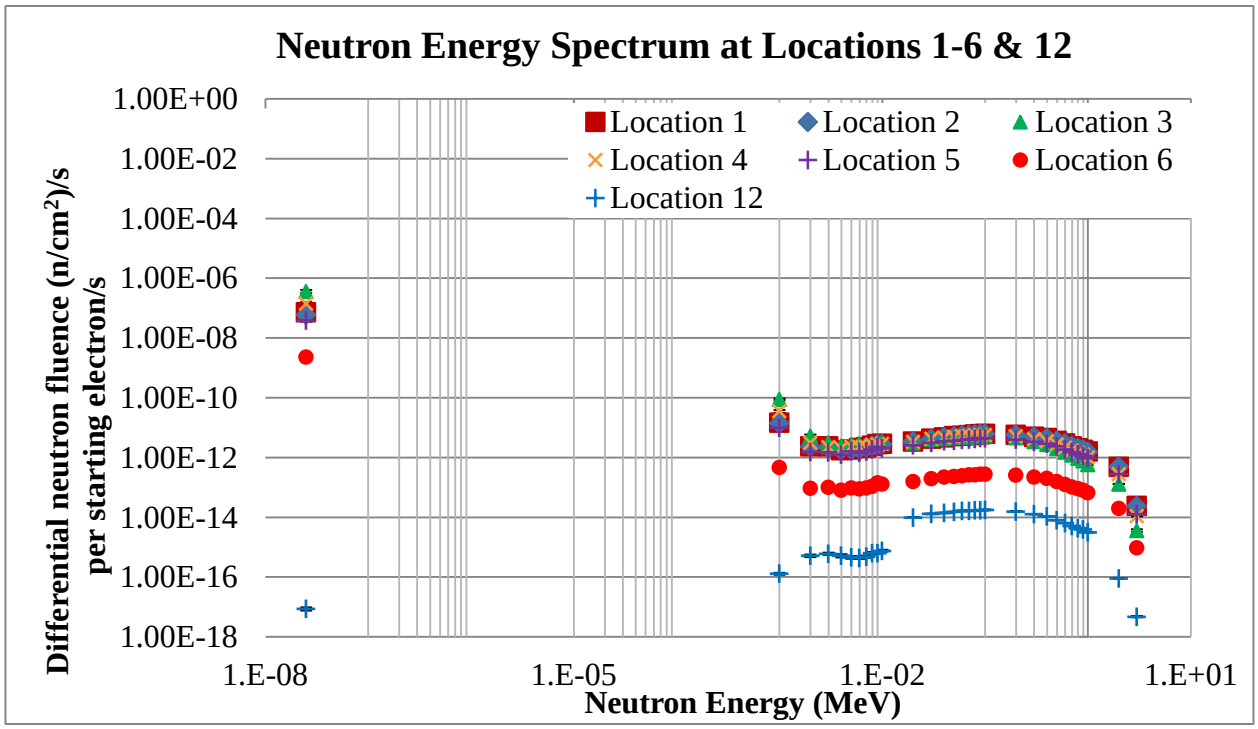

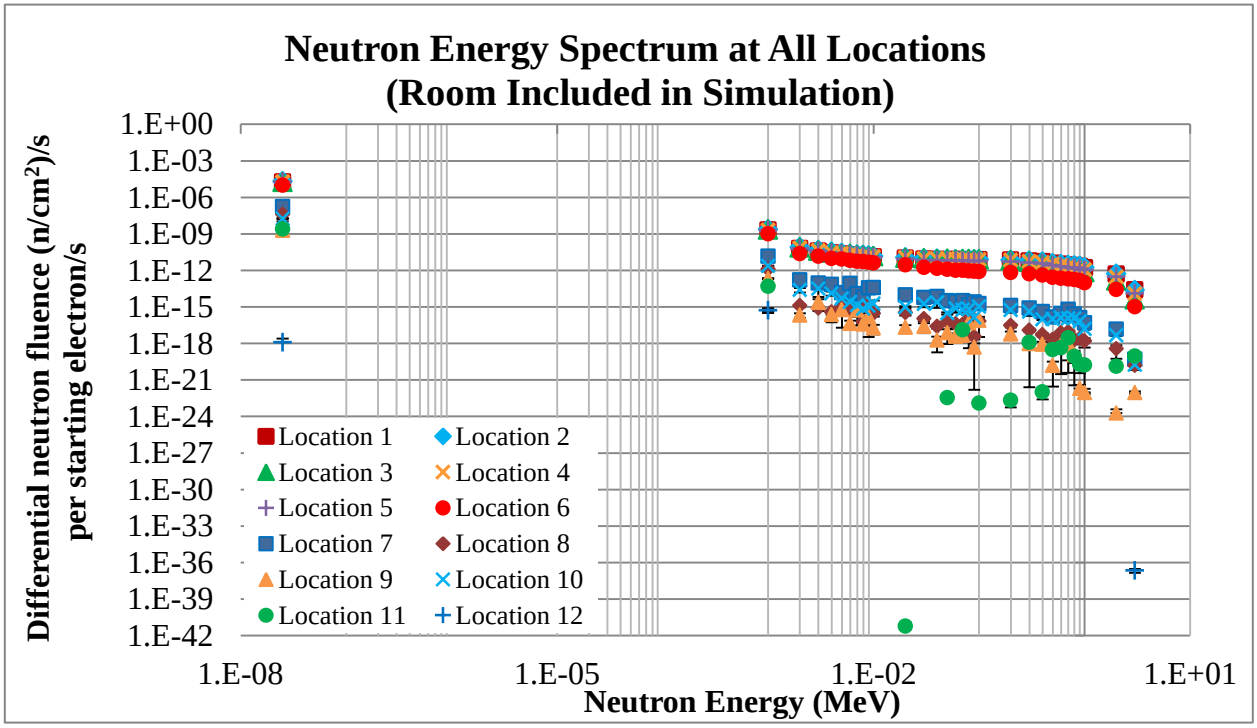

Figure 15. Simulation 4 neutron spectrum.
Locations 1-6 and 12 (Top). All locations with surrounding room (Bottom).

MCNP Electron Beam Simulation

Table 10 summarizes the neutron yield at the selected linac components for the electron mode, and Figure 16 shows the accompanied neutron energy spectrum obtained. Table 11 summarizes the neutron fluence and dose rates at the point detectors selected for Simulation 6 and Table 12 shows these results normalized to electron Gy at the isocenter. The location numbers listed in Tables 11 and 12 are representative of the positions listed in Table 6. Figure 17 summarizes the neutron energy spectra for simulation 6.

Table 10. Simulation 5 Results

Linac Component (Material)	**Neutron Yield/s per Starting Electron/s**	**MCNP5 Relative Error**
Primary Scattering Foil (Ta)	3.78×10^{-6}	0.13
Secondary Scattering Foil (Al)	1.16×10^{-5}	0.11
Jaws (W)	1.28×10^{-3}	0.05
Electron Applicator (Zinc Alloy)	4.69×10^{-5}	0.43

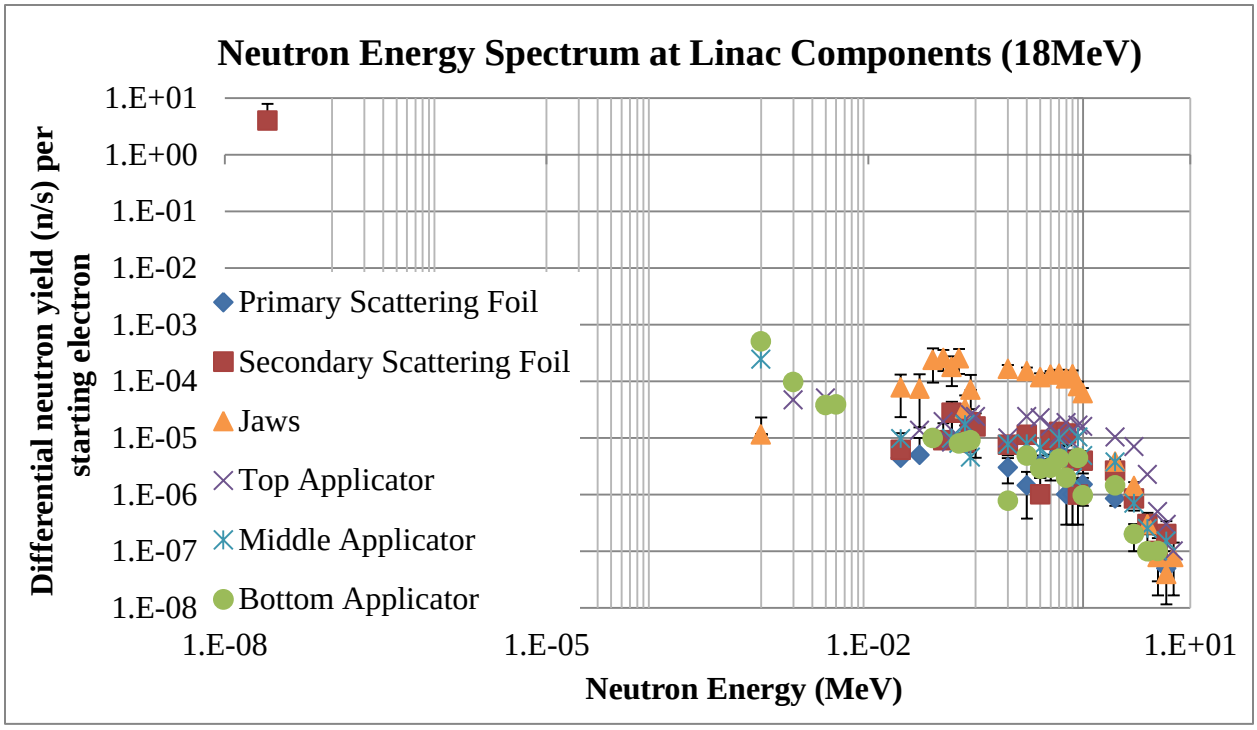

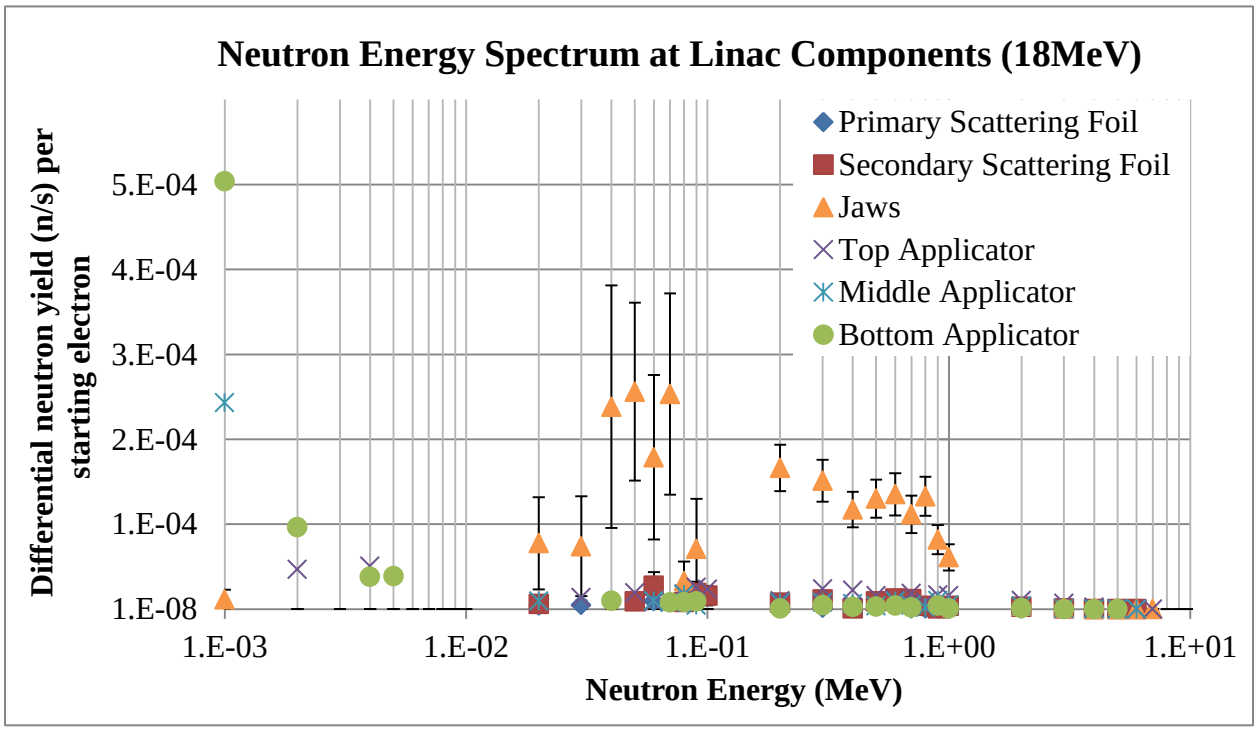

Figure 16. Simulation 5 neutron spectrum.
Entire spectrum (Top). Spectrum excluding thermal energy portion (Bottom).

Table 11. Simulation 6 Results

Location	Neutron Fluence (n/cm^2)/s per starting electron/s	Relative Error	Neutron Dose Rate (mrem/h) per starting electron/s	Relative Error
Locations below include the linac and phantom in the model only				
Isocenter (IC)	2.03×10^{-8}	0.145	1.03×10^{-9}	0.060
Location 1	5.38×10^{-9}	0.005	3.95×10^{-10}	0.058
Location 2	5.38×10^{-9}	0.006	4.78×10^{-10}	0.066
Location 3	1.35×10^{-8}	0.006	1.10×10^{-9}	0.051
Location 4	9.72×10^{-9}	0.005	7.82×10^{-10}	0.048
Location 5	4.65×10^{-9}	0.005	3.78×10^{-10}	0.050
Location 6	2.66×10^{-10}	0.005	2.13×10^{-11}	0.055
Location 12	5.39×10^{-11}	0.011	3.52×10^{-12}	0.040
Locations below include the surrounding room in the model				
Isocenter (IC)	1.32×10^{-8}	0.0651	1.28×10^{-9}	0.0725
Location 1	9.87×10^{-9}	0.012	5.02×10^{-10}	0.004
Location 2	1.03×10^{-8}	0.012	5.20×10^{-10}	0.004
Location 3	1.83×10^{-8}	0.015	1.16×10^{-9}	0.004
Location 4	1.46×10^{-8}	0.014	8.51×10^{-10}	0.004
Location 5	9.42×10^{-9}	0.012	4.42×10^{-10}	0.004
Location 6	2.22×10^{-9}	0.029	4.46×10^{-11}	0.004
Location 7	2.22×10^{-11}	0.161	1.98×10^{-13}	0.203
Location 8	2.83×10^{-12}	0.235	5.17×10^{-14}	0.564
Location 9	2.34×10^{-13}	0.339	2.05×10^{-15}	0.249
Location 10	6.21×10^{-12}	0.164	5.95×10^{-14}	0.071
Location 11	5.18×10^{-15}	0.406	3.13×10^{-15}	0.452
Location 12	3.15×10^{-30}	0.757	4.58×10^{-17}	0.986

Table 12. Normalized to electron Gy delivered at the isocenter

Location	Neutron Fluence (n/cm^2) per electron Gy	Neutron Dose (mrem) per electron Gy
Locations below include the linac and phantom in the model only		
Isocenter (IC)	1.15×10^{10}	1.63×10^{5}
Location 1	3.06×10^{9}	6.24×10^{4}
Location 2	3.06×10^{9}	7.55×10^{4}
Location 3	7.68×10^{9}	1.74×10^{5}
Location 4	5.53×10^{9}	1.23×10^{5}
Location 5	2.65×10^{9}	5.97×10^{4}
Location 6	1.52×10^{8}	3370
Location 12	3.07×10^{7}	540
Locations below include the surrounding room in the model		
Isocenter (IC)	7.51×10^{9}	2.02×10^{5}
Location 1	5.62×10^{9}	7.94×10^{4}
Location 2	5.89×10^{9}	8.22×10^{4}
Location 3	1.04×10^{10}	1.83×10^{5}
Location 4	8.30×10^{9}	1.35×10^{5}
Location 5	5.36×10^{9}	6.99×10^{4}
Location 6	1.26×10^{9}	7050.37
Location 7	1.27×10^{7}	31.32
Location 8	1.61×10^{6}	8.18
Location 9	1.33×10^{5}	0.32
Location 10	3.53×10^{6}	9.41
Location 11	2.95×10^{3}	0.50
Location 12	1.71×10^{-12}	0.01

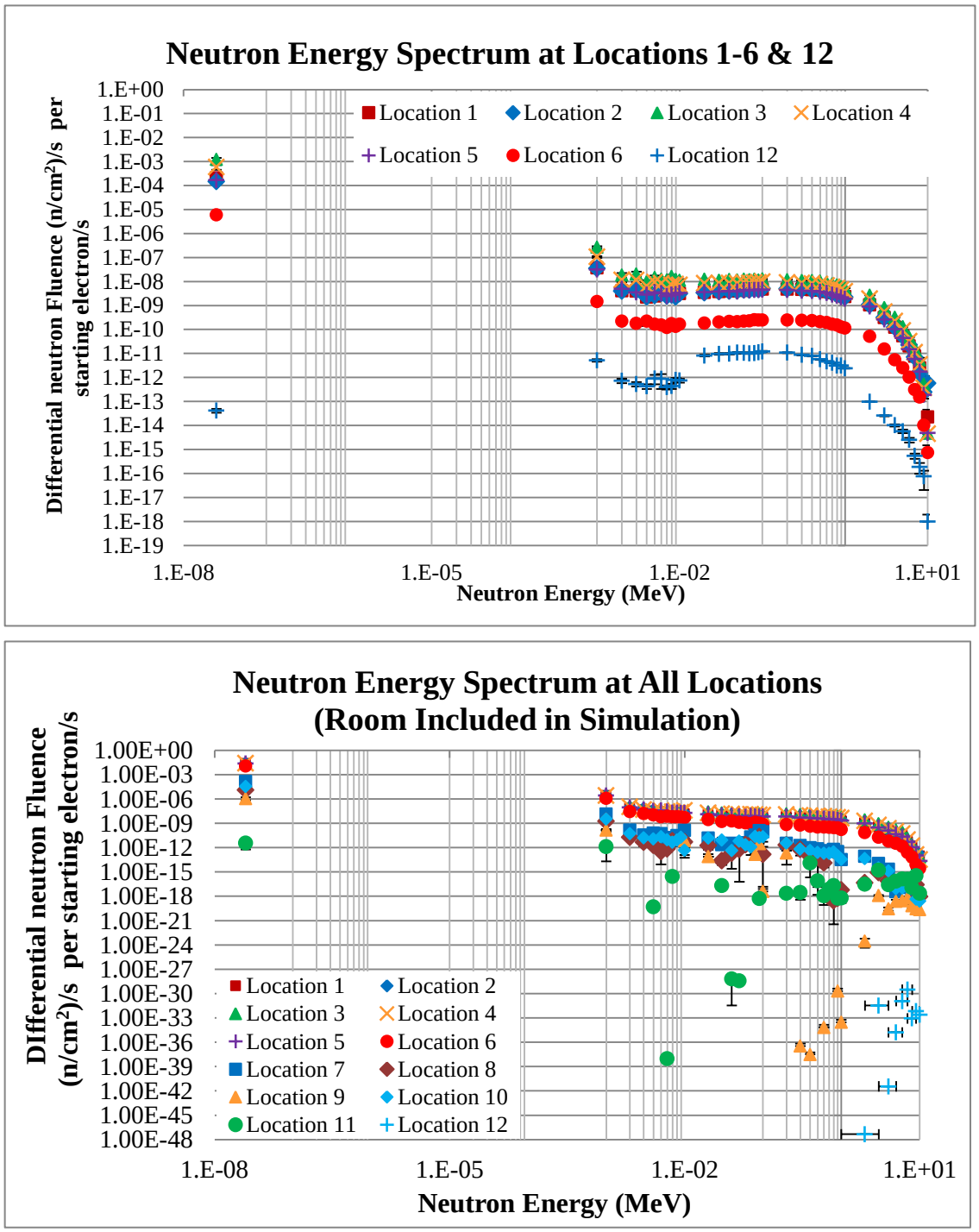

Figure 17. Simulation 6 neutron spectrum.
Locations 1-6 and 12 (Top). All locations with surrounding room (Bottom).

MCNP Results with Adjusted Jaws and MLCs

As mentioned in the introduction, the upper and lower jaws are used to create a square field size at the isocenter. Up to this point, the simulations included geometries for the upper jaws and lower jaws that were not quite representative of the jaws for the VTH machine. An appropriate representation includes upper jaws along the x-axis and lower jaws along the y-axis. Further, when the machine is set to deliver a 10 x 10 cm^2 field size at the isocenter for the photon mode and IMRT is not used (as in this study), the MLCs are open and not collimated as they were in the above simulations. Also, for the electron mode, though MLCs are not used with this mode, they are still present in the geometry and fully open, thus they cannot be completely ignored in the simulation. To correct for the jaws and the MLCs, Simulations 4b and 6b were repeated, but with the correct x and y jaws and open MLCs in the geometry. Table 13 summarizes the results (normalized to photon and electron Gy at the isocenter) for both modalities.

Table 13. Simulations 4b and 6b results with corrected jaws and MLCs

Location	Neutron dose (mrem) per photon Gy (Photon Mode)	Uncertainty (mrem/photon Gy)	Neutron dose (mrem) per electron Gy (Electron Mode)	Uncertainty (mrem/photon Gy)
Locations below include the linac and phantom in the model only				
Isocenter (IC)	71.21	12.03	1.03×10^{5}	7193
Location 1	224.95	0.88	6.23×10^{4}	5915
Location 2	223.22	0.94	6.19×10^{4}	5575
Location 3	347.81	1.53	1.57×10^{5}	2.22×10^{4}
Location 4	274.27	1.10	1.14×10^{5}	2.22×10^{4}
Location 5	161.27	0.61	6.10×10^{4}	5642
Location 6	11.77	0.05	4108	314
Location 12	3.09	0.02	556	106
Locations below include the surrounding room in the model				
Isocenter (IC)	63.85	18.18	1.38×10^{5}	5.59×10^{4}
Location 1	262.15	2.12	3.94×10^{4}	1.17×10^{4}
Location 2	268.21	1.61	4.96×10^{4}	1.44×10^{4}
Location 3	426.54	4.69	1.77×10^{5}	6.34×10^{4}
Location 4	337.34	3.04	1.15×10^{5}	3.26×10^{4}
Location 5	199.86	1.14	6.67×10^{4}	1.53×10^{4}
Location 6	25.35	0.23	1.72×10^{4}	8150
Location 7	0.087	0.009	12.56	12.56
Location 8	0.010	0.004	2.78	2.78
Location 9	0.001	0.0002	8.82×10^{-5}	8.82×10^{-5}
Location 10	0.015	0.003	15.69	15.69
Location 11	0.0008	0.0006	0.12	0.12
Location 12	3.34×10^{-6}	3.34×10^{-6}	1.10×10^{-16}	1.10×10^{-16}

Also included in this section (see Table 14) are the photon doses at locations 8 to 11 as these are the locations where occupational exposures are likely to occur. These photon doses are used to determine the difference between photon and neutron exposure for radiation safety purposes.

Table 14. MCNP photon dose at specified locations for both modalities

Location	Photon dose (mrem) per photon Gy (Photon Mode)	Uncertainty (mrem/photon Gy)	Photon dose (mrem) per electron Gy (Electron Mode)	Uncertainty (mrem/photon Gy)
Location 8	0.024	0.011	77.71	53.79
Location 9	0.001	0.0002	4.39	2.12
Location 10	0.087	0.016	19.59	8.72
Location 11	0.034	0.014	43.53	25.07

Physical Experiment

Tables 15 and 16 summarize the results of the physical experiment data for both modalities. These results include the gamma dose rates that were generated with MCNP at each location. The neutron dose rates reported in both tables include gamma rejection using the MCNP model as well as the leakage mentioned in the material and methods, and the energy response corrections of 0.023 (for the photon mode) and 0.049 (for the electron mode). Again, these dose rates only account for the neutron energies of 0.2 MeV and above.

Table 15. Physical measurements for the 10 MV photon beam

Location	MCNP gamma dose rate (mrem/h)	MCNP Uncertainty (mrem/h)	Neutron dose rate (mrem/h)	Corrected Measurement Uncertainty (mrem/h)
1	3.33×10^{6}	$\pm 1.05 \times 10^{5}$	41.86	± 12.66
2	3.33×10^{6}	$\pm 1.04 \times 10^{5}$	44.08	± 11.62
3	2.89×10^{7}	± 1.17 x 106	26.04	± 40.31
4	1.29×10^{7}	$\pm 5.66 \times 10^{5}$	35.98	± 21.36
5	3.22×10^{6}	$\pm 1.24 \times 10^{5}$	38.80	± 10.83
6	2.41×10^{5}	$\pm 1.33 \times 10^{4}$	4.65	± 1.10
7	171	± 51.3	0.08	± 0.11
8	3.32	± 0.85	0	± 0.11
9	0.579	± .39	0	± 0.10
10	40	± 11.6	0	± 0.11
11	11.5	± 5.01	0	± 0.10
12	1.08×10^{-7}	$\pm 7.95 \times 10^{-8}$	0.085	± 0.10
12 (no room)	3100	± 171	0.087	± 0.10

Table 16. Physical measurements for the 18 MeV electron beam

Location	MCNP gamma dose rate (mrem/h)	MCNP Uncertainty (mrem/h)	Neutron dose rate (mrem/h)	Corrected Measurement Uncertainty (mrem/h)
1	6.84×10^{7}	$\pm 2.39 \times 10^{6}$	0	± 79
2	8.73×10^{7}	$\pm 1.56 \times 10^{7}$	0	± 520
3	1.50×10^{9}	$\pm 1.20 \times 10^{8}$	0	± 3987
4	7.66×10^{8}	$\pm 7.76 \times 10^{7}$	0	± 2585
5	2.04×10^{8}	$\pm 2.14 \times 10^{7}$	0	± 712
6	1.03×10^{7}	$\pm 172 \times 10^{6}$	0	± 57
7	197	± 508	0.069	± 0.12
8	1160	± 507	0	± 0.10
9	197	± 1.77	0	± 0.10
10	636	± 154	0	± 0.10
11	2150	± 723	0	± 0.10
12	2.9×10^{-5}	± 9.07 x 10-^{6}	0	± 0.14
12 (no room)	1.20×10^{5}	$\pm 11.1 \times 10^{4}$	0.121	± 0.40

Analysis and Discussion

For both modalities, the MCNP results (specifically for the isocenter, and locations in the room) were different for the simulations with just the linac model versus the simulations that included the room surrounding the linac. This shows the influence that the surrounding walls have on the neutron distribution and, ultimately, neutron dose. The comparison of the neutron doses for both modalities with and without the room is obvious in Figure 18. The surrounding walls result in slightly elevated doses. A t-test was performed and confirmed that the differences are statistically significant (greater than 3 standard deviations).

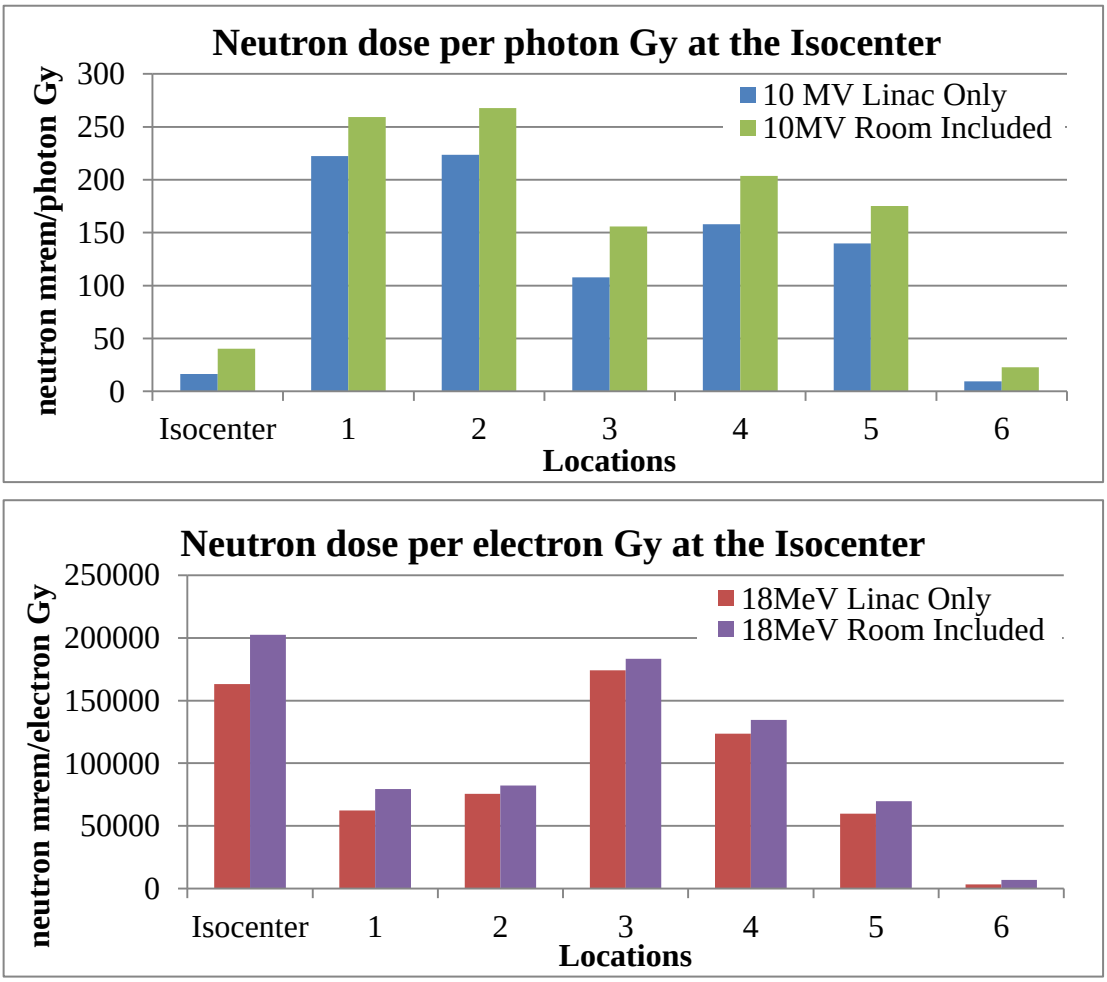

Figure 18. Comparison of MCNP results with and without the surrounding room. 10 MV photon mode (Top). 18 MeV electron mode (Bottom)

Photon Modality

From examination of the energy spectrum, the jaws are the biggest contributor to neutron production. This is actually the case for both modalities, but for the purpose of discussion, the photon mode is analyzed. This is consistent with the literature as can be seen in Table 17 and makes sense considering that the jaws are made of tungsten which has a threshold of 7.4 MeV for photoneutron production. MCNP Simulation 3 results (neutron yield at the linac components) are compared to results from the literature (Liu et al., 1997) in Table 17.

Table 17. MCNP simulation 3 compared to the literature

Linac Component (Material)	**MCNP n/s per starting electron**	**(Liu et al., 1997) EGS4-MORSE n/s per starting electron**
Target (Cu)	5.13×10^{-10}	1.70×10^{-9}
Primary Collimator (W)	2.39×10^{-7}	5.90×10^{-6}
Flattening Filter (Cu)	8.66×10^{-9}	4.50×10^{-9}
Jaws (W)	1.03×10^{-6}	7.30×10^{-6}

As can be seen, there is an order of magnitude difference between the values for the target and primary collimator. One reason for the difference could be the different measurement conditions between the MCNP modeling in this study and that of the literature, specifically at the target. Even so, the difference in modeling at the source doesn't make as big of a difference at the flattening filter and jaws. As seen in Table 17, the values are similar. Also similar is the fact that the jaws show the highest yield. Adjusting the jaws and MLCs did not make a big difference in the comparisons.

Locations 1-4 for Simulation 4a are compared to values in the literature (Liu et al., 1997) as well. Table 18 shows the comparisons. Interestingly for this comparison, unlike the

component yields, the MCNP values from this research are larger by one to two orders of magnitude.

Table 18. MCNP simulation 4a compared to the literature

Location	MCNP $n/cm^2/s$ per photon Gy at IC	(Liu et al, 97) EGS4-MORSE $n/cm^2/s$ per photon Gy at IC
1	1.25×10^7	2.4×10^5
2	1.25×10^7	2.4×10^5
3	7.69×10^7	3.0×10^5
4	9.81×10^6	8.7×10^4

Though the MCNP values are larger, an important observation to be made is that there is a similar progression at each location. The fluence is highest at location 3 and lowest at 4, etc. The influencing factor is anticipated to be originating from a difference in geometries of the linac components. For this research, assumptions were made regarding the geometries and, to some extent the material, of the linac components. These assumptions could have resulted in further disparity in the readings.

MCNP Simulation 4 results (with the corrected jaw and MLC geometry) are compared with the physical measurement results (see Table 19). To accurately compare the two, neutron energies 0.2 MeV to 10 MeV from the MCNP results are included in Table 19 only and not the entire spectrum. The percent errors, specifically for the first six locations are reasonable if the physical measurements are compared to the MCNP simulation with only the linac modeled. With the room included, surprisingly the doses at locations 1-6 are lower and a comparison cannot be made. An explanation for this is that the energies below 0.2 MeV specifically when the surrounding room is factored in contribute more to the dose than energies between 0.2 and 10 MeV. In either case, the MCNP readings are lower.

Table 19. Comparison of photon beam MCNP simulation and physical experiment

Experiment Locations	MCNP Simulation (mrem/photon Gy)	Physical Measurements (mrem/photon Gy)	Percent Error of MCNP compared to Measurements
Locations below (for MCNP) include the linac and phantom in the model only			
1	0.093	0.133	30%
2	0.112	0.140	20%
3	0.017	0.082	79%
4	0.046	0.114	60%
5	0.082	0.123	33%
6	0.007	0.015	53%
12 (no ceiling)	0.005	2.69×10^{-4}	---
Locations below (for MCNP) include the surrounding room in the model			
1	4.88×10^{-4}	0.133	---
2	4.78×10^{-4}	0.140	---
3	5.67×10^{-4}	0.082	---
4	5.40×10^{-4}	0.114	---
5	2.50×10^{-4}	0.123	---
6	7.07×10^{-6}	0.015	---
7	2.02×10^{-9}	2.79×10^{-4}	---
8	1.86×10^{-11}	0	---
9	5.27×10^{-12}	0	---
10	1.32×10^{-9}	0	---
11	1.70×10^{-12}	0	---
12	1.34×10^{-27}	2.77×10^{-4}	---

One last comparison to demonstrate for the photon modality is the difference in neutron doses for the original geometry compared to the simulations with the corrected jaws and MLCs. A t-test was performed to determine if the differences are statistically significant. As can be seen in Table 20, locations in the room showed statistically significant differing values. This emphasizes the importance of accurate beam geometry in MCNP modeling. An important observation to make is that there is no statistical significance at the locations of concern where occupational exposures are likely to occur (locations 8-11).

Table 20. Comparison of MCNP with different jaw and MLC geometry (photon mode)

Locations	Neutron dose (mrem/photon Gy) with original geometry	Neutron dose (mrem/photon Gy) with correct geometry	t-test (number of standard deviations)
Locations below (for MCNP) include the linac and phantom in the model only			
IC	16.38	71.21	4.46
1	222.47	224.95	2.45
2	223.64	223.22	0.38
3	107.83	347.81	150.36
4	157.96	274.27	94.668
5	139.82	161.27	30.40
6	9.60	11.77	40.67
12	3.48	3.09	15.54
Locations below (for MCNP) include the surrounding room in the model			
IC	40.38	63.85	1.20
1	259.12	262.15	1.38
2	267.67	268.21	0.32
3	155.71	426.54	56.94
4	203.71	337.34	42.85
5	175.05	199.86	20.72
6	22.75	25.35	10.06
7	0.088	0.087	0.02
8	0.007	0.010	0.88
9	0.001	0.001	0.38
10	0.016	0.015	0.35
11	0.001	0.0008	0.27
12	0	3.34×10^{-6}	0.67

Electron Modality

No data were found in the literature review to compare the electron beam results, thus only the MCNP and physical measurements from this study are compared. The hope is that results from this work can be used in future experiments where neutron production is evaluated for electron beam modalities.

MCNP Simulation 6 results (with the corrected jaw and MLC geometry) are compared with the physical measurement results for the electron mode. Just as with the photon mode, to accurately compare the two, neutron energies 0.2 MeV to 10 MeV from the MCNP results are

included in Table 21 only. As can be seen, there is such a large difference between the MCNP values and the physical measurements. This is not surprising considering the large uncertainty for the physical measurements.

Table 21. Comparison of electron beam MCNP simulation and physical experiment

Experiment Locations	MCNP Simulation (mrem/electron Gy)	Physical Measurements (mrem/electron Gy)	Percent Error of MCNP compared to Measurements
Locations below (for MCNP) include the linac and phantom in the model only			
1	10.50	0	---
2	14.88	0	---
3	10.61	0	---
4	12.19	0	---
5	11.05	0	---
6	1.19	0	---
12	0.13	3.83×10^{-04}	---
Locations below (for MCNP) include the surrounding room in the model			
1	0.069	0	---
2	0.083	0	---
3	0.630	0	---
4	0.318	0	---
5	0.101	0	---
6	0.005	0	---
7	7.45×10^{-07}	2.17×10^{-04}	---
8	6.28×10^{-07}	0	---
9	1.67×10^{-07}	0	---
10	2.64×10^{-11}	0	---
11	2.64×10^{-11}	0	---
12	1.10×10^{-16}	0	---

Just as for the photon mode, a comparison was made for the electron mode to demonstrate the difference in doses for the original geometry compared to the simulations with the corrected jaws and MLCs. Table 22 demonstrates whether the differences are considered statistically significant or not. Interestingly for the electron mode, the doses are not as statistically significant. One explanation for this could be the higher uncertainties seen in MCNP modeling with the electron mode.

Table 22. Comparison of MCNP with different jaw and MLC geometry (electron mode)

Locations	Neutron dose (mrem/electron Gy) with original geometry	Neutron dose (mrem/electron Gy) with correct geometry	t-test (number of standard deviations)
Locations below (for MCNP) include the linac and phantom in the model only			
IC	1.63×10^{5}	1.03×10^{5}	4.92
1	6.24×10^{4}	6.23×10^{4}	0.02
2	7.55×10^{4}	6.19×10^{4}	1.81
3	1.74×10^{5}	1.57×10^{5}	0.73
4	1.23×10^{5}	1.14×10^{5}	0.68
5	5.97×10^{4}	6.10×10^{4}	0.20
6	3370	4108	2.03
12	540	556	0.13
Locations below (for MCNP) include the surrounding room in the model			
IC	2.02×10^{5}	1.38×10^{5}	1.12
1	7.94×10^{4}	3.94×10^{4}	3.43
2	8.22×10^{4}	4.96×10^{4}	2.26
3	1.83×10^{5}	1.77×10^{5}	0.08
4	1.35×10^{5}	1.15×10^{5}	0.61
5	6.99×10^{4}	6.67×10^{4}	0.21
6	7050.37	1.72×10^{4}	1.25
7	31.32	12.56	1.33
8	8.18	2.78	1.0
9	0.32	8.82×10^{-5}	4.01
10	9.41	15.69	0.40
11	0.50	0.12	1.49
12	0.01	1.10×10^{-16}	1.01

Implications of Results to Patient and Occupational Exposure

An important consideration to be made when evaluating neutron dose is exposure to the patient from the treatment beam and to the staff from the photons that have leaked out from the tube head (or are scattered off of the walls in the room) and penetrate through the shielding. Regardless of the presence of neutrons in the various locations and the high differences in the comparisons in this study, there is a photon presence as well that could arguably be considered significantly higher than the neutron dose.

For the patient, the question is whether the neutron doses are even remotely close to the 1 Gy (100,000 mrem for photons and electrons) that is delivered at the isocenter for both modalities. For the photon mode, the neutron dose is considerably lower by a factor of over 1000, thus for the photon mode the neutron dose to the patient could be considered negligible compared to the treatment dose. For the electron mode, the neutron dose is almost the same as the electron dose at the isocenter, thus the neutron dose cannot be considered negligible. As for occupational exposures, Table 23 shows the neutron doses versus the photon doses at Locations 8-11 where occupational exposures are likely to occur.

Table 23. MCNP photon doses versus neutron doses at specified locations

Location	Photon dose (mrem) per photon Gy (Photon Mode)	Neutron dose (mrem) per photon Gy (Photon Mode)	Photon dose (mrem) per electron Gy (Electron Mode)	Neutron dose (mrem) per electron Gy (Electron Mode)
Location 8	0.024	0.010	77.71	2.78
Location 9	0.001	0.001	4.39	8.82×10^{-5}
Location 10	0.087	0.015	19.59	15.69
Location 11	0.034	0.0008	43.53	0.12

For the photon mode, the difference between photon and neutron doses at locations 8 and 9 is not very great, thus the neutron doses cannot be considered negligible (compared to the photon dose) at these locations. However, the difference for locations 10 and 11 are high enough (a factor of 5 for location 10, and a factor of over 40 for location 11), that the dose from neutrons can be considered negligible. For the electron mode, with exception of location 10, all locations have photon doses considerably higher than the neutron doses, thus the neutron dose from these locations could be considered negligible. Though the neutron dose is considered non-negligible compared to the photon dose in some of the locations listed in Table 23, the overall limits for

radiation safety should be considered. For occupational workers, the annual limit is 5,000 mrem (Johnson and Birky, 2012). Considering that the 10 MV photon beam is only used once per week and the electron mode is rarely, if ever, used at the VTH, the neutron doses listed in Table 23 can be considered negligible as they do not even approach even 1% of the 5,000 mrem annual limit for occupational workers.

Limitations and Recommendations for Future Work

There are several limitations that should be addressed concerning this study, and most likely can explain the large differences observed when comparing MCNP versus the measured results. First, uncertainty in beam geometry is a big limiting factor. Though uncertainties can be accounted for with MCNP, this is only one side of the coin. Geometry is modeled based on limited information provided by the manufacturer. Thus, assumptions were made in this study with several dimensions and shapes as well as the materials of the components. As demonstrated in the results, one of these assumptions was corrected and shows the influence different beam geometries have on neutron doses. Further, geometries are not the same across machines. The machine studied at the VTH is different than machines evaluated in the literature. For example, each is calibrated differently. Thus, uncertainties that cannot be quantified can lead to less precise geometries in MCNP modeling, and most definitely contribute to differences when comparing the literature data and physical measurements.

Second, a lot of uncertainty resulted from using the BF_3 detector because of the limitations of the neutron energy range measured as well as the high gamma interference. Because of the limits of the detector, for both modalities only the neutron energies between 0.2 and 10 MeV at the linac from the MCNP modeling were compared with physical measurements. Thus, the dose contribution from thermal neutrons as well as neutrons with energies between

thermal and 0.2 MeV is unknown and an accurate representation of the true dose from all neutrons produced was not available to compare with MCNP results. Regarding gamma interference, because such a high gamma field is present at the locations in the room in particular, this could be interfering with the meter readings. Thus, even though the MCNP comparison versus the physical measurements were more reasonable for locations 1-5 (photon beam only), these numbers may not be accurate. A better representation of the measureable dose equivalent can be obtained with instruments, such as bubble dosimeters or activation foils. A brief description of each is provided in Appendix E.

Lastly, this experiment only involved one dose, field size, and gantry position condition. In the literature (Catchpole, 2010), the field sizes at the isocenter were varied, and this influenced the neutron yield. Varying the delivered dose to the isocenter and changing the gantry angle will influence neutron yield and direction as well. To better evaluate the neutron yield and dose at the VTH linac, an extended and refined analysis considering the above parameters for both the photon and electron modality is recommended.

Conclusion

In conclusion, for both the 10 MV photon beam and the 18 MeV electron beam, MCNP results, and physical measurements with a large uncertainty, showed neutron production. Areas simulated and measured include locations in and outside the linac room with both MCNP and physical measurements made with a BF_3 neutron dose rate meter with a moderator sphere sensitive to neutron energies between 0.2 and 10 MeV. For the photon mode, MCNP modeling resulted in measurable neutron dose equivalents per photon Gy up to 0.112 mrem/photon Gy, and physical measurements up to 0.133 mrem/photon Gy. For the electron mode, MCNP modeling resulted in measureable neutron dose equivalents per electron Gy up to 14.88 mrem/electron Gy, and physical measurements up to 3.83×10^{-04} electron Gy. Taking the entire neutron spectrum into account, MCNP results showed neutron doses up to 347.81 mrem/ photon Gy at the isocenter for the photon beam, and up to 1.77×10^{5} mrem/electron Gy at the isocenter for the electron beam. The conclusion made from this research is that neutrons are generated at various locations in and outside the room. For the photon modality, the neutron dose to the patient can be considered negligible when compared with the treatment dose. For both modalities, neutron doses are far below the occupational limits for radiation workers, thus the neutron production does not appear to exceed the tolerance for workers in appropriate locations surrounding the VTH linac vault. Due to the limitations addressed in this study, further research is recommended for an accurate assessment of both modalities. Recommendations include varying field sizes, delivered doses, and gantry angles as well as using bubble dosimeters or activation foils to physically measure the neutron dose (from the entire neutron spectrum) more accurately.

References

Attix, F. H. *Introduction to Radiological Physics and Radiation Dosimetry*. WILEY-VCH, 2004.

Catchpole, M. E. *Comparison of Secondary Neutron Dose from 10MV Intensity Modulated Radiation Therapy and Volume Modulated Arc Therapy.* MS Thesis. Oregon State University, Corvallis, 2010. Web. 31 Jan 2013

Cember, H., and Johnson, T. E. *Introduction to Health Physics, 4th ed*. McGraw Hill Medical, 2009.

National Council on Radiation Protection and Measurements (1984). Neutron Contamination from Medical Electron Accelerators: Recommendations of the National Council on Radiation Protection and Measurements. Bethesda, MD.

National Council on Radiation Protection and Measurements (2005). Structural Shielding Design and Evaluation for Megavoltage X- and Gamma-Ray Radiotherapy Facilities: Recommendations of the National Council on Radiation Protection and Measurements. Bethesda, MD.

Agosteo, S., Foglio, P. A., Maggioni, B. "Neutron fluxes in radiotherapy rooms". *Medical Physics*. March 1993;20(2 Pt 1):407-414.

Barquero, R., Edwards, T., Iñiguez, M., and Vega-Carrillo, H. "Monte Carlo simulation estimates of neutron doses to critical organs of a patient undergoing 18 MV x-ray LINAC-based radiotherapy". *Medical Physics*. December 2005;32(12):3579-3588.

Deye, J. A., and Young, F. D. "Neutron production from a 10 MV medical linac". *Phys. Med. Biol.* 1997;22:90.

Facure, A., da Silva, A., da Rosa, L., Cardoso, S., and Rezende, G. "On the production of neutrons in laminated barriers for 10 MV medical accelerator rooms". *Medical Physics*. July 2008;35(7):3285-3292.

Howell, R., Kry, S., Burgett, E., Hertel, N., and Followill, D. "Secondary neutron spectra from modern Varian, Siemens, and Elekta linacs with multileaf collimators". *Medical Physics*. September 2009;36(9):4027-4038.

Johnson, T.E., and Birky, B.K. *Health Physics and Radiological Health, 4th ed*. Wolters Kluwer/Lippincott Williams & Wilkins: (2012).

Khan, F. M. *The Physics of Radiation Therapy, 4th ed*. Wolters Kluwer/Lippincott Williams & Wilkins: (2010).

Knoll, G. F. *Radiation Detection and Measurement, 4th ed.* John Wiley & Sons, Inc: (2010)

Lin, J., Chu, T., Lin, S., and Liu, M. "The measurement of photoneutrons in the vicinity of a Siemens Primus linear accelerator". *Applied Radiation And Isotopes: Including Data, Instrumentation And Methods For Use In Agriculture, Industry And Medicine*. September 2001;55(3):315-321.

Liu, J. C., Kase, K. R., Mao, X. S., Nelson, W. R., Kleck, J. H., and Johnson, S. "Calculations of Photoneutrons from Varian Clinac Accelerators and Their Transmissions in Materials". *Presented at Radiation Dosimetry and Safety, Taipei, Taiwan.* 1997.

Lo, Y. "Albedos for 4-, 10-, and 18-MV bremsstrahlung x-ray beams on concrete, iron, and lead--normally incident". *Medical Physics*. May 1992;19(3):659-666.

Mao, X., Kase, K., Liu, J., Nelson, W., Kleck, J., and Johnson S. "Neutron sources in the Varian Clinac 2100C/2300C medical accelerator calculated by the EGS4 code". *Health Physics*. April 1997;72(4):524-529.

McGinley, P. H., and Sohrabi, M. "Neutron contamination in the primary beam". *Proceeding of a Conference on Neutrons from Electron Medical Accelerators,* NBS Special Publication 554, Heaton H. T., and Jacobs R., Eds. (US Government Printing Office, Washington). 1979.

McGinley, P. H., Wood, M., Mills M., and Rodriguez, R. "Dose levels due to neutrons in the vicinity of high-energy medical accelerators". *Medical Physics*. 1976;3:397.

Oliver, G. D. (1976) Revised data from "Fast neutron contamination in x-ray beams of medical accelerators from 19 to 45 MV," presented at the annual meeting of the American Association of Physicists in Medicine (1974).

Turner, J.E. *Atoms, Radiation, and Radiation Protection.* WILEY-VCH, 2007.

Varian Medical Systems. (2013). Monte Carlo Data Package High Energy Accelerator. Retrieved from https://varian.force.com/

X-5 Monte Carlo Team. *MCNP—A General Monte Carlo N-Particle Transport Code, Version 5, Volume II: User's Guide*. Los Alamos, NM, Los Alamos National Laboratory. 2003.

Appendix A

MCNP5 source definition and energy bins selected for photon beam simulation

```
sdef pos=0 0 .54 erg=d1 vec=0 0 -1 dir=d2 par=2 $ see nsimg1 notes
si1 h 0 .01 .02 .03 .04 .05 .06 .07 .08 .09 .1 .2 .3 .4 .5 .6 .7 .8 .9 1 2 3 &
4 5 6 7 8 9 10 $ cut at 10 MeV for now
sp1 d 0 0.1381 0.0170 0.0454 0.0823 0.1658 0.4285 0.5384 0.7756 1.0657 1.2932 &
1.4711 1.0683 0.7469 0.5675 0.4726 0.3677 0.3130 0.2626 0.2294 0.1313 &
 0.05936 0.0328 0.0199 0.0121 0.0074 0.0042 0.0019 0.0004 $ used results (differential from
184mebeamsource
sb1 d 0 .01 .01 .01 .01 .01 .01 .01 .01 .01 .01 .01 .01 .01 .01 .01 .01 .01 &
.01 .01 .01 .01 .01 .01 .01 .2 .2 .4 .4 $ for rescaling energies
si2 -1 0.9635 1
sp2 0 0 1
```

Appendix B

Designer and Manufacturer of Scientific and Industrial Instruments

CERTIFICATE OF CALIBRATION

LUDLUM MEASUREMENTS, INC.
501 Oak Street, Sweetwater, TX 79556, U.S.A., 325-235-5494
☐ 10744 Dutchtown Road, Knoxville, TN 37932, U.S.A., 865-392-4601

CUSTOMER COLORADO STATE UNIVERSITY ORDER NO. 20227587/395059

Mfg. Ludlum Measurements, Inc. Model 12-4 Serial No. 118950

Mfg. Ludlum Measurements, Inc. Model 42-31 Serial No. PR 133726

Cal. Date 6-Aug-13 Cal Due Date 6-Aug-14 Cal. Interval 1 Year Meterface 202-477

Check mark ☑ applies to applicable instr. and/or detector IAW mfg. spec. T. 75 °F RH 47 % Alt 698.8 mm Hg

☐ New Instrument Instrument Received ☑ Within Toler. +-10% ☐ 10-20% ☐ Out of Tol. ☐ Requiring Repair ☐ Other-See comments

☑ Mechanical ck. ☑ Meter Zeroed ☐ Background Subtract ☑ Input Sens. Linearity
☑ F/S Resp. ck ☑ Reset ck. ☐ Window Operation ☑ Geotropism
☑ Audio ck. ☐ Alarm Setting ck. ☑ Batt. ck. (Min. Volt) 2.2 VDC
☐ Calibrated in accordance with LMI SOP 14.8 rev 12/05/89. ☑ Calibrated in accordance with LMI SOP 14.9 rev 02/07/97.

Instrument Volt Set 1727 V Input Sens. 2 mV Det. Oper. 1727 V at 2 mV Threshold Dial Ratio = mV

☑ HV Readout (2 points) Ref./Inst. 500 / 501 V Ref./Inst. 2000 / 2000 V

COMMENTS:
Gamma rejection <10cpm at 10R/hr for Cs137.

Gamma Calibration: GM detectors positioned perpendicular to source except for M 44-9 in which the front of probe faces source.

RANGE/MULTIPLIER	REFERENCE CAL. POINT	INSTRUMENT REC'D "AS FOUND READING"	INSTRUMENT METER READING*
X1000	240,000 cpm	8	8
X1000	60,000 cpm	2	2
X100	800mrem/hr = 24,000 cpm	8	8
X100	200mrem/hr	2	2
X10	80mrem/hr	8	8
X10	20mrem/hr	2	2
X1	8mrem/hr	8	8
X1	2mrem/hr	2	2

*Uncertainty within ± 10% C.F. within ± 20%

X1000 **Range(s) Calibrated Electronically**

	REFERENCE CAL. POINT	INSTRUMENT RECEIVED	INSTRUMENT METER READING*
Digital Readout			
Log Scale			

Ludlum Measurements, Inc. certifies that the above instrument has been calibrated by standards traceable to the National Institute of Standards and Technology, or to the calibration facilities of other International Standards Organization members, or have been derived from accepted values of natural physical constants or have been derived by the ratio type of calibration techniques. The calibration system conforms to the requirements of ANSI/NCSL Z540-1-1994 and ANSI N323-1978

State of Texas Calibration License No. LO-1963

Reference Instruments and/or Sources: ☐ 059 ☐ 280 ☐ 720 ☐ 734 ☐ 781 ☐ 1131 ☐ 1616 ☐ 1696 ☐ 5105 ☐ 5717CO ☐ 5719CO
☐ 60646 ☐ 70897 ☐ 73410 ☐ E551 ☐ E552 ☐ G112 ☐ M565 ☐ S-394 ☐ S-1054 ☑ T-304 ☐ T879 ☐ T10081 ☐ T10082 ☐ Y982

☐ Alpha S/N ☐ Beta S/N ☐ Other

☑ m 500 S/N 130362 ☐ Oscilloscope S/N ☑ Multimeter S/N 78401031

Calibrated By: [signature] Date 6-Aug-13

Reviewed By: [signature] Date 7Aug13

This certificate shall not be reproduced except in full, without the written approval of Ludlum Measurements, Inc.
FORM C22A 02/26/2013 Page 1 of 1

AC Inst. Only ☐ Passed Dielectric (Hi-Pot) and Continuity Test ☐ Failed:

Appendix C

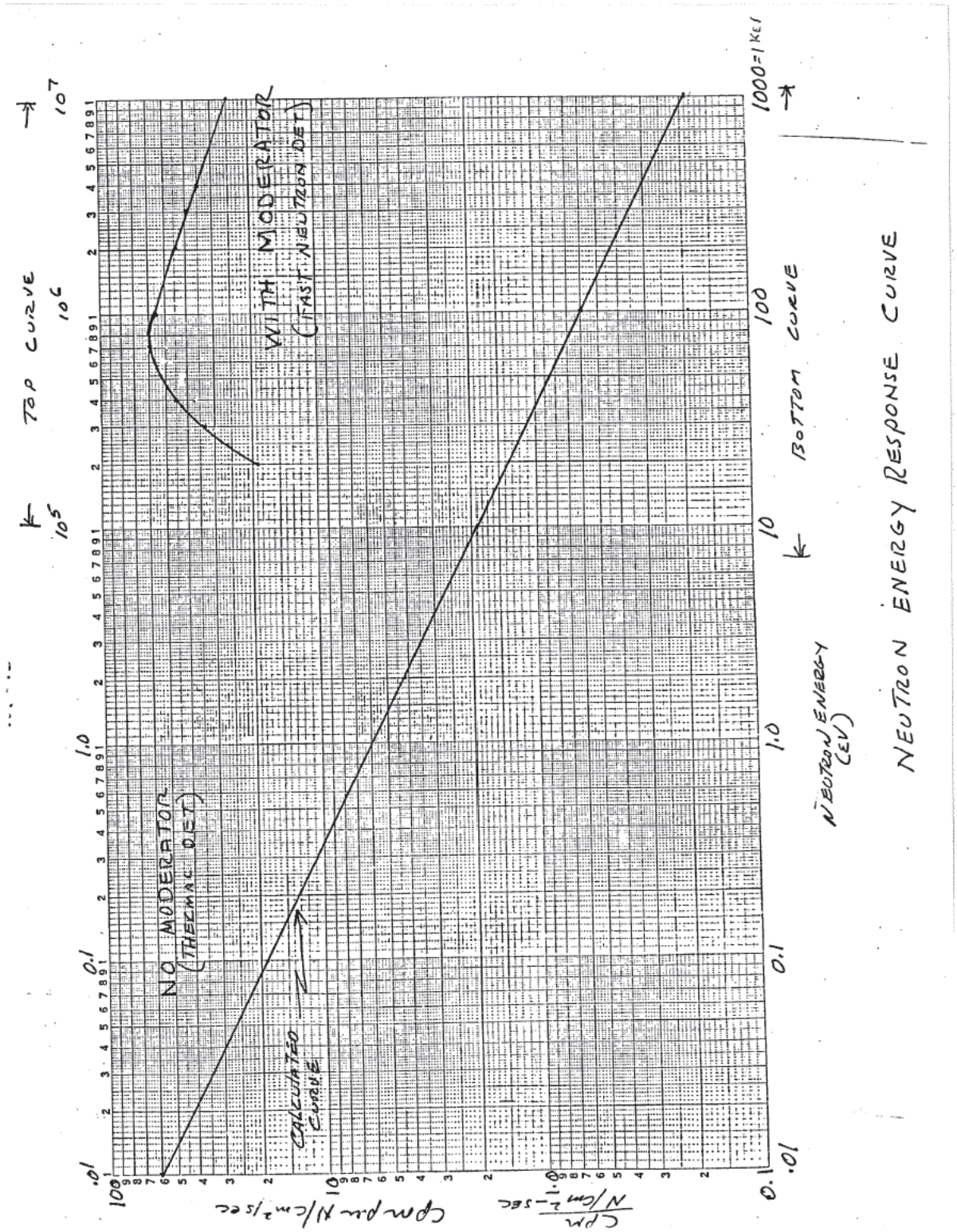
NEUTRON ENERGY RESPONSE CURVE
NEUTRON ENERGY (EV)
BOTTOM CURVE
TOP CURVE
1000=1 KEV
NO MODERATOR (THERMAL DET)
WITH MODERATOR (FAST NEUTRON DET)
CALCULATED CURVE
CPM PER N/cm²-SEC
CPM PER N/cm²/SEC

Appendix D

Determination of Correction Factor used in the physical measurement results and analysis.

The AmBe source spectrum in the table below is from Figure 7.5.1 of Health Physics and Radiological Health (Johnson, 2012). Location 1 for the 10 MV photon beam spectra is used as the example for how the correction factor of 0.023 was derived. The same concept was used to determine the 0.049 correction factor for the 18 MeV electron beam as well.

Energy (MeV)	AmBe neutron cpm per cm^2/s	Normalized AmBe $n/cm^2/s$	Normalized Spectrum at Linac $n/cm^2/s$	Ration Between Linac and AmBe Source Spectra	Linac neutron cpm per cm^2/s	Location 1 cpm at each Energy	cpm per E/ neutron cpm per cm^2/s
						*1933 mrem/h = 58000cpm	
0.20	19	0.022	0.191	2.814	53	3591	67
0.30	35	0.04	0.166	1.343	47	3116	66
0.40	45	0.04	0.148	1.199	54	2782	52
0.50	52	0.07	0.120	0.553	29	2246	78
0.60	56	0.07	0.097	0.450	25	1826	73
0.70	59	0.07	0.079	0.363	21	1476	69
0.80	60	0.07	0.069	0.318	19	1292	68
0.90	59	0.07	0.061	0.280	17	1139	69
1.00	56	0.07	0.053	0.243	14	987	73
2.00	45	0.25	0.016	0.021	1	304	322
3.00	39	0.25	0.001	0.001	53	15	372
						Total cpm	1307
						Actual mrem/h	43.58
						Correction	0.023

*Based on the Certificate of Calibration in Appendix B, the assumption was made that there is a linear relationship between cpm and mrem/h with a slope of 30 (see figure below). This relation is used in the above table.

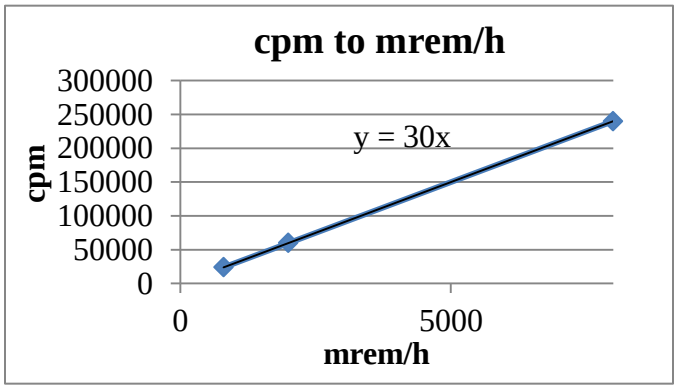

Appendix E

Bubble Dosimeters

Bubble dosimeters consist of fluid droplets (in a superheated state) suspended in an inert matrix. When a neutron interacts in the matrix, charged particles are produced. These charged particles deposit energy locally in the matrix and cause the superheated droplets to burst into bubbles that can be seen with the human. The bubbles (calibrated to a certain number of bubbles per dose) are counted. As the droplets in the matrix are insensitive to the electrons that are produced by gamma ray interactions, these dosimeters are insensitive to gamma radiation. The bubble dosimeters can be made sensitive to thermal and intermediate neutrons by introducing elements that have high cross sections for each neutron type. Thus, doses from various neutron energies can be assessed. (Knoll, 2010)

Activation Foils

Activation foils are very tiny wires of materials that have high cross section for different neutron interactions: (n,γ) for thermal, (n,p) for fast. The neutrons induce radioactivity that can be counted. The measured radiation is used to deduce information (i.e. neutron numbers and energies) about the neutrons. Examples of materials ideal for evaluating thermal neutrons include Manganese, Copper, and Gold. Examples of materials ideal for evaluating fast neutrons include Nickel, Zinc, and Indium. (Knoll, 2010)